DOKUZ EYLÜL UNIVERSITY
GRADUATE SCHOOL OF NATURAL AND APPLIED SCIENCES

EXPERIMENTAL INVESTIGATION OF LOCAL SCOUR AROUND THE HEAD SECTION OF THE RUBBLE MOUND BREAKWATER IN CASE OF BREAKING WAVES

by
Yusuf YAŞIR

December, 2022
İZMİR

EXPERIMENTAL INVESTIGATION OF LOCAL SCOUR AROUND THE HEAD SECTION OF THE RUBBLE MOUND BREAKWATER IN CASE OF BREAKING WAVES

A Thesis Submitted to the
Graduate School of Natural and Applied Sciences of Dokuz Eylül University
In Partial Fulfillment of the Requirements for the Degree of Master of Science in Civil Engineering, Hydraulic, Hydrology and Water Resources Program

by
Yusuf YAŞIR

December, 2022
İZMİR

M.Sc THESIS EXAMINATION RESULT FORM

We have read the thesis entitled **"EXPERIMENTAL INVESTIGATION OF LOCAL SCOUR AROUND THE HEAD SECTION OF THE RUBBLE MOUND BREAKWATER IN CASE OF BREAKING WAVES"** completed by **YUSUF YAŞIR** under supervision of **ASSOC. PROF. DR. MUSTAFA DOĞAN** and we certify that in our opinion it is fully adequate, in scope and in quality, as a thesis for the degree of Master of Science.

…………………………………

Assoc. Prof. Dr. Mustafa DOĞAN

Supervisor

…………………………. …………………………….......................

Prof. Dr. Özlem TERZİ — Jury Member

Assoc. Prof. Dr. Ayşegül Özgenç AKSOY — Jury Member

Prof. Dr. Okan FISTIKOĞLU

Director

Graduate School of Natural and Applied Sciences

ACKNOWLEDGMENTS

First, I would like to give my deepest thanks to my supervisor Assoc. Prof. Dr. Mustafa Doğan, has always been with me in my thesis and academic studies. He has a great contribution to my choice of specialization field and my academic progress.

Also, I am grateful to my dear wife for always standing with me throughout my thesis study. She motivated me during the writing of the thesis and was patient when I couldn't have spare time for her.

Thanks to the Scientific and Technological Research Council of Turkey (TUBITAK) for supporting the study through the project number 218M445 and the project name "Experimental and numerical investigation of local ground movements in the trunk and head sections of rubble-mound breakwaters under the influence of regular and irregular waves"

Yusuf YAŞIR

EXPERIMENTAL INVESTIGATION OF LOCAL SCOUR AROUND THE HEAD SECTION OF THE RUBBLE MOUND BREAKWATER IN CASE OF BREAKING WAVES

ABSTRACT

Coastal structures and anchored vessels can be damaged by the effect of waves. In order to minimize these damages, long embankments called breakwaters are built to form a calm water level. The breakwaters absorb the energy of the wave before it reaches the shore, therefore reducing the wave height on the shore. However, in the trunk and head sections of these structures, scour and deposition can occur with the effect of waves and currents. And as a result of the scour, stability problems and damages, to the point of collapsing, can be seen. For this reason, it is very important to examine the scour that occurs around the breakwater. Although there are existing studies on the head section for non-breaking waves, no experimental study examines the local scour under the effect of breaking waves. Therefore, this thesis aims to eliminate deficiency in the literature and to examine the local scour that may cause stability losses in the breakwater for the breaking wave case. In this study, the local scour in the head section of a rubble mound breakwater under the effect of the breaking waves was experimentally investigated. The experiments were carried out for two different bed materials (0.23 mm and 0.55 mm) and five different regular waves (1.7 s, 2.0 s, 2.3 s, 2.7 s, 3.1 s). In this thesis, the breaking and non-breaking wave cases were compared and as a result, it was concluded that the scour significantly reduced for the breaking case. In the experiments carried out under the breaking wave conditions, no significant local scour was observed in either bed material conditions.

Keywords: Rubble mound breakwater, head section, breaking and non-breaking waves, local scour, experimental study.

KIRILAN DALGALAR DURUMUNDA ŞEVLİ YÜZLÜ DALGAKIRAN KAFA KESİTİNDEKİ YEREL OYULMALARIN DENEYSEL ARAŞTIRILMASI

ÖZ

Kıyı yapıları ve demirlenmiş halde bulunan gemiler, dalgaların etkisiyle zarar görebilir. Bu zararları en aza indirmek için dalgakıran adı verilen uzun setler inşa edilerek sakin bir su seviyesi oluşturulur. Dalgakıranlar, dalganın enerjisini kıyıya ulaşmadan sönümleyerek kıyıdaki dalga yüksekliğini azaltır. Ancak bu yapıların gövde ve kafa kısımlarında dalga ve akıntıların etkisiyle oyulma ve yığılma meydana gelebilir. Oyulma sonucunda ise stabilite sorunları ve göçmelere varan hasarlar görülebilmektedir. Bu nedenle dalgakıran çevresinde oluşan oyulmanın incelenmesi oldukça büyük önem taşımaktadır. Kırılmayan dalgalar için kafa kesiti ile ilgili çalışmalar olmasına rağmen, kırılan dalgaların etkisi altındaki yerel oyulmayı inceleyen herhangi bir deneysel çalışma bulunmamaktadır. Bu nedenle bu tez çalışması, literatürdeki eksikliği gidermeyi ve kırılan dalga durumu için dalgakıranda stabilite kayıplarına neden olabilecek yerel oyulmayı incelemeyi amaçlamaktadır. Bu çalışmada, kırılan dalgaların etkisi altında bir şevli yüzlü taş dolgu dalgakıranın kafa kesitindeki yerel oyulma deneysel olarak incelenmiştir. Deneyler, iki farklı taban malzemesi (0.23 mm ve 0.55 mm) ve beş farklı düzenli dalga (1.7 s, 2.0 s, 2.3 s, 2.7 s, 3.1 s) için gerçekleştirilmiştir. Bu tezde, kırılan ve kırılmayan dalga durumları karşılaştırılmış ve sonuç olarak kırılma durumu için oyulmanın önemli ölçüde azaldığı sonucuna varılmıştır. Kırılmış dalga koşullarında gerçekleştirilen deneylerde, her iki taban malzemesi durumunda önemli bir yerel oyulma gözlemlenmemiştir.

Anahtar Kelimeler: Şevli yüzlü dalgakıran, kafa kesiti, kırılan ve kırılmayan dalgalar, yerel oyulma, deneysel çalışma.

CONTENTS

LIST OF FIGURES

Page

LIST OF TABLES

Pages

CHAPTER ONE
INTRODUCTION

Our country which is surrounded by seas on three sides needs coastal structures in parallel with the economic development in recent years. Among these structures, coastal protection structures have an important place. Coastal protection structures absorb wave energy before it reaches the shore, creating a calm water level in coastal areas. In this way, activities such as trade, transportation and fishing can be carried out properly on the shore. These structures may be breakwaters, seawalls, groins, jetties, dikes, bulkheads, etc. Breakwaters are the most built coastal protection structure in our country and the world. They create a calm water level on the shore, creating a safe area for anchored vessels.

Breakwaters can be divided into many classes according to their shapes, the materials they are made of, their purpose of use, and their appearance in the plan. Foremost among them, the rubble-mound breakwater is the most built in our country and the world. One of the important factors that make rubble-mound breakwaters to be preferred is that the stone material to be used in construction of rubble-mound breakwater is close to construction site which means lower construction costs. Additively, another advantage of rubble-mound breakwaters is that it significantly reduces wave energy with the help of their inclined and voided structure.

The construction process of breakwater structures might be very costly. Therefore, it is important to determine the optimum materials and dimensions while remaining at acceptable reliability levels during the design phase. In addition, stability losses caused by the scour can lead to significant repair cost increases in coastal structures. Hence, it is important to eliminate the elements that may disrupt the stability of coastal structures with high engineering knowledge in terms of reducing costs. The risk of the scour causing stability losses around coastal structures makes the scour a phenomenon worth examining.

Breakwaters built on erodible seabed are subjected to waves and currents. As a result of the effect of waves and currents, scour occurs around breakwaters. When scour reaches considerable levels, it can disrupt the stability of the breakwater. Therefore, research on the local scour in the head section of breakwaters has great importance. In the literature, scour studies are divided into two trunk and head section. Only a limited number of scour studies can be found. Those studies especially examined the trunk section. There is no any experimental study examining local scour on the head section for breaking wave case in the literature. For this reason, this study aims to fill the gap in the literature.

Within the scope of this study, the local ground movements that occur due to the regular wave effect on the head section of the rubble-mound breakwater for breaking wave case were experimentally investigated. The experiments were carried out in an existing open-wave channel in the Hydraulics Laboratory of Dokuz Eylül University, Civil Engineering Department. A model breakwater head was created in the channel. Time-dependent variation of the scour on the head section of the breakwater for the breaking wave case, was experimentally investigated.

In the thesis, the scour caused by steady streaming and plunging breaker were examined separately for the breaking and non-breaking cases under the same conditions. In case of the breaking wave case, there was 47.07 percent decrease in the final scour depth caused by steady streaming, while there was 81.82 percent decrease in the final scour depth caused by the plunging breaker. The experiments were performed in seabed materials with median grain diameters of 0.55 mm and 0.23 mm, wave periods of 1.7 s, 2.0 s, 2.3 s, 2.7 s, 3.1 s, and a slope of 1:1.5. No significant scour depth has been observed as a result of the experiments.

CHAPTER TWO
MECHANICS OF SCOUR

The mechanics of the scour causing stability losses in the coastal structures have been the subject of researchers. The researchers have conducted experimental studies to able to understand the mechanics of the scour. As a result of these studies, the parameters affecting the scour have been revealed. In this section, the general terms and parameters used in the literature related to scour are explained.

2.1 General Information and Definitions

There are two main parameters used in scour studies: equilibrium scour depth and time scale of scour. Equilibrium scour depth is a name that is given to the scour depth that has become balanced. In other words, it is the depth of scour at which a considerable amount of the scour occurs. The time which takes for most of the scour to occur is called the time scale of scour. The equation of time-dependent scour depth is given in (2.1).

$$S_t = S \left(1 - \exp\left(-\frac{t}{T}\right)\right) \tag{2.1}$$

where

S_t: time-dependent scour depth at any time t.

S: equilibrium scour depth

T: time scale of scour

Scour at the toe of a rubble-mound breakwater occurs in two different stages as scour progress and equilibrium stage. Figure 2.1 demonstrates the temporal progress of scour depth. As given in Fig. 2.1, time scale, T, can be obtained by drawing a tangent to the curve or taking integral of the area above the curve.

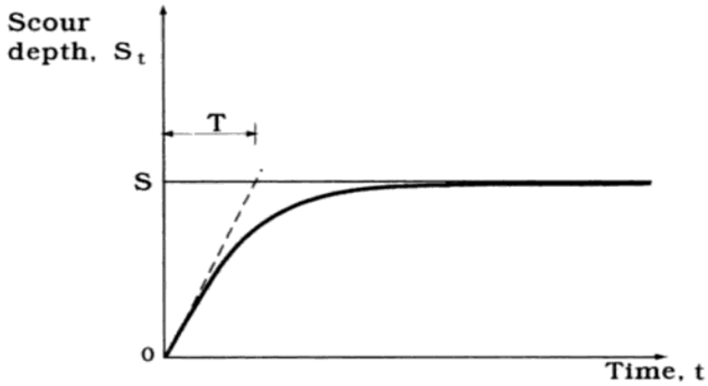

Figure 2.1 Change in scour depth with time

A parameter called Shields (θ) is frequently used in scour studies. The Θ is an effect value for the sediments to be activated. Furthermore, scour can be divided into clear water and live-bed scour. The θ is used to understand if the scour is clear-water or live-bed scour. The undisturbed Shields parameter is defined as follows:

$$\theta = \frac{{U_f}^2}{(g*(s-1)*d_{50})} \tag{2.2}$$

where U_f, undisturbed bed shear velocity, g, acceleration due to gravity, d_{50}, median grain diameter, s, specific gravity of sediment grains. Equation 2.2 is valid for the only steady current case. In case of waves, U_f transforms into maximum friction velocity, U_{fm}. The U_{fm} is calculated as below:

$$U_{fm} = \sqrt{\frac{f_w}{2}}U_m \tag{2.3}$$

where

f_w: wave friction coefficient

U_m: maximum undisturbed orbital velocity at the seabed

While there is no sediment motion at a certain distance from the coastal structure in case of clear-water scour ($\theta<\theta_{cr}$), in case of live-bed scour, sediment transport is also observed at far distances from the coastal structure ($\theta>\theta_{cr}$). There is a different parameter called the critical Shields parameter, θ_{cr}, which is used in the literature. The θ_{cr} is used to specify if there is clear-water or live-bed scour. It indicates the critical value required to initiate sediment movement on the seabed and varies depending on the grain Reynolds number, $(d_{50*}U_f)/\nu$. For $\theta<\theta_{cr}$, clear-water scour is observed, while in case of $\theta>\theta_{cr}$, live-bed scour is observed. In Fig. 2.2, while sediment movement is observed in the upper part of the line, it is not observed in the lower part. The data demonstrated in Fig. 2.2 is compiled by Yalin and Karahan (1979).

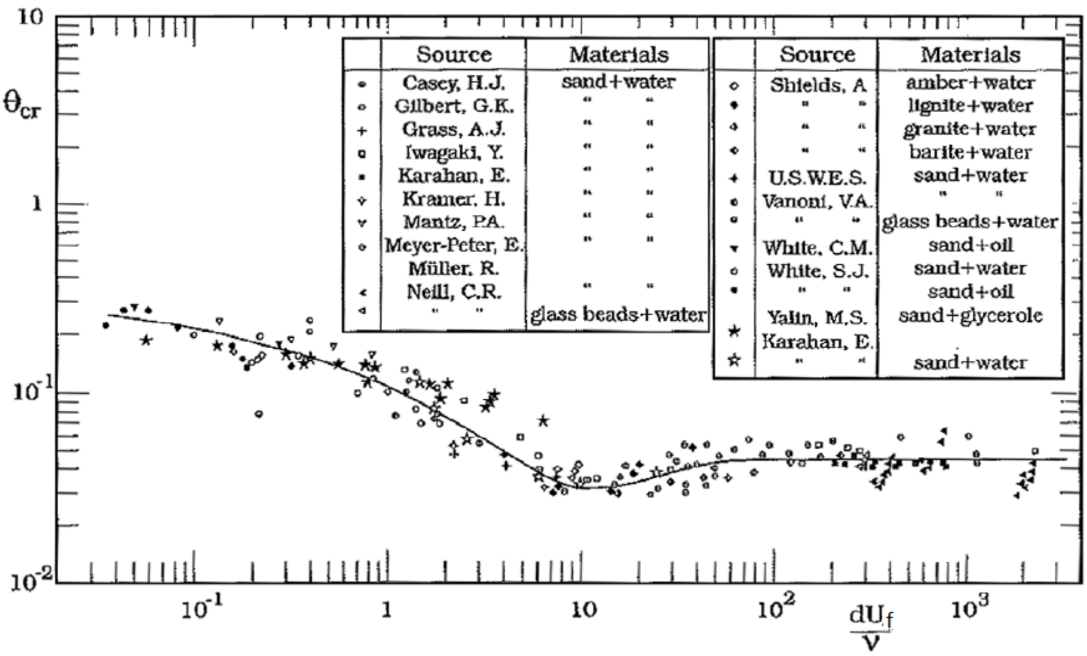

Figure 2.2 Beginning of grain movement on the seabed (Sumer and Fredsøe, 2002)

Soulsby and Whitehouse (1997) expressed the θ_{cr} as in equation 2.4.

$$\theta cr = \frac{0.30}{1+1.2D_*} + 0.055(1 - \exp(-0.02D_s)) \quad (2.4)$$

with D* as the non-dimensional grain diameter:

$$D_* = d\left[\frac{\left(\frac{\rho_s}{\rho}-1\right)g}{v^2}\right]^{1/3} \quad (2.5)$$

Scour mainly takes place around coastal structures as a result of the effect of waves and currents. When a structure is located in sea, it increases sediment transport around itself because it disrupts the flow structure. As a result, the existence of the structure will lead to an increment in the bed shear stress and the turbulence level. In other words, an increment in the bed shear stress near the coastal structure will cause an increment in scour depth, and the increase in the bed shear stress is denoted by the amplification factor, α, in the literature. It is defined for the head section as below:

$$\alpha = \frac{max|\tau|}{\tau_m} \quad (2.6)$$

where

τ: bed shear stress

τ_m: maximum undisturbed bed shear stress

The amplification factor decreases with distance from the structure. Since, as you move away from the structure, the deterioration in the structure of the flow decreases. It means lower bed shear stress. The α decreases in huge amounts in the event of rubble-mound breakwater. The α increased up to 14 for the vertical-wall breakwater, while the α can be decreased by a factor of seven in the event of the rubble-mound breakwater. Indeed, this is a big decrease in the α. The decrease in the α is related to geometric structure of the breakwater because wave energy is absorbed over inclined breakwater surface. The deterioration of flow structure close to the head section will be decreased eventually. This situation consequently leads to a substantial decrease in the α at the head of the rubble-mound breakwater. Figure 2.3 demonstrates the variation of the amplification factor around the head section. As seen in Fig. 2.3, the α takes a maximum of three. As mentioned above, the α decreases as you move away from the breakwater.

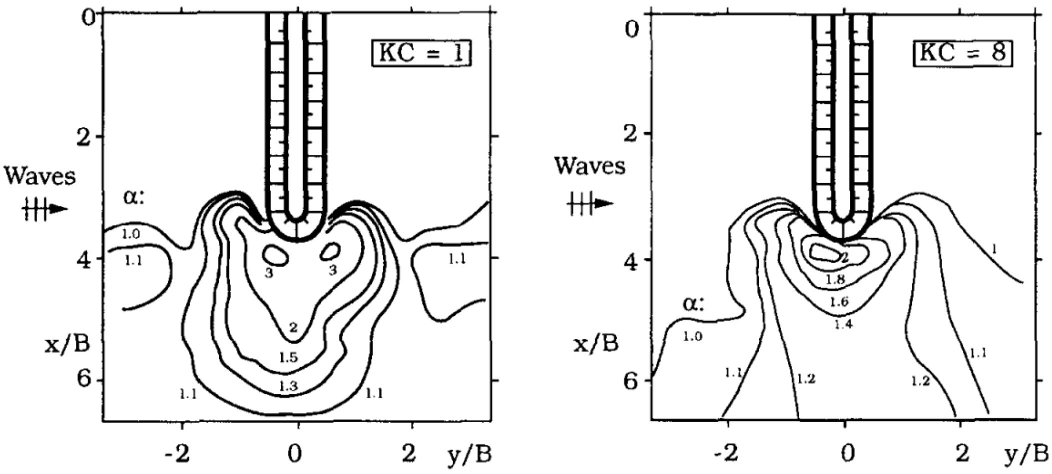

Figure 2.3 Variation of the amplification factor around the breakwater head. Side slope: 1:1. Fredsøe and Sumer (1997)

When it comes to the wave effect, a different non-dimensional parameter called Keulagen Carpenter number, *KC,* which affects the scour was encountered. It describes the ratio of drag forces to inertia forces. As a physical expression, *KC* number is expressed as the ratio of the length of the movement area of the moving fluid particles to the base width of the breakwater for the scour caused by steady streaming as given in equation 2.7. For the scour caused by plunging breaker, the denominator, *B,* turns to wave height, *H,* as in equation 2.8.

$$KC = \frac{U_m T_w}{\mathrm{B}} \quad (2.7)$$

$$KC = \frac{U_m T_w}{\mathrm{H}} \quad (2.8)$$

where

U_m: the maximum undisturbed orbital velocity at the seabed

T_w: wave period

B: base width of the breakwater

H: wave height

The form of *KC* varies from structure to structure. For example, the denominator *B* turns to diameter, *D*, for pipelines and piles while the sediment-ripple length, L_r, for the trunk section.

2.2 Dimensional Analysis

Dimensional analysis helps to understand the process followed to reach a solution. While doing this, it uses the dimensional variables in the problem. Dimensional analysis allows the solution of many engineering problems. Dimensionless variables are obtained with the help of dimensional variables, and it provides a more understandable presentation of the experimental results. First, the dimensional parameters affecting the event are determined and dimensionless parameters are written in terms of dimensional parameters. To do this, two different methods are used: Rayleigh and Buckingham – π. In this thesis, dimensional analysis is done using the Buckingham – π. When applying this method, U_m, ρ, and *B* are determined as repeated dimensional quantities.

Dimensional parametres affecting the examined experimental study are listed as below:

Parameters belonging to flow: U_m, g, T_w, H, h, L

Parameters belonging to fluid: ρ, μ

Parameters belonging to bed: ρ_s, d_{50}

Geometrical parameters: B, S

The first dimensionless number is obtained as the Reynolds number given by equation 2.14.

$$\pi_1 = U_m^a \rho^b B^c \mu^1 \tag{2.9}$$

$$K^0 L^0 T^0 = (LT^{-1})^a (KL^{-4}T^2)^b L^c (KL^{-2}T)^1 \tag{2.10}$$

$$K \rightarrow 0 = b + 1 \rightarrow b = -1 \tag{2.11}$$

$$L \rightarrow 0 = a - 4b - 2c + 1 \rightarrow c = -1 \tag{2.12}$$

$$T \rightarrow 0 = 2b + c - a = 0 \rightarrow a = -1 \tag{2.13}$$

$$\pi_1 = U_m^{-1} \rho^{-1} B^{-1} \mu^1 = \frac{\mu}{U_m \rho B} = \frac{\nu}{U_m B} = Re_D^{-1} \tag{2.14}$$

Similarly, other dimensionless quantities can be obtained respectively; Keulegan-Carpenter number (2.20), dimensionless seabed grain median diameter (2.26), relative scour depth (2.32), seabed relative specific gravity (2.38), relative wavelength (2.44), Froude number (2.50), relative wave height (2.56), relative water depth (2.62).

$$\pi_2 = U_m^a \rho^b B^c T_w^1 \tag{2.15}$$

$$K^0 L^0 T^0 = (LT^{-1})^a (KL^{-4}T^2)^b L^c (T)^1 \tag{2.16}$$

$$K \rightarrow 0 = b \ \rightarrow b = 0 \quad (2.17)$$

$$L \rightarrow 0 = a - 4b + c \rightarrow c = -1 \quad (2.18)$$

$$T \rightarrow 0 = 2b + c - a = 0 \rightarrow a = +1 \quad (2.19)$$

$$\pi_2 = U_m^{\ 1} \rho^0 B^{-1} T_w^{\ 1} = \frac{U_m \ T_w}{B} = KC \quad (2.20)$$

$$\pi_3 = U_m^{\ a} \rho^b B^c d_{50}^{\ 1} \quad (2.21)$$

$$K^0 L^0 T^0 = (LT^{-1})^a (KL^{-4}T^2)^b L^c (L)^1 \quad (2.22)$$

$$K \rightarrow 0 = b \ \rightarrow b = 0 \quad (2.23)$$

$$L \rightarrow 0 = a - 4b + c + 1 \rightarrow c = -1 \quad (2.24)$$

$$T \rightarrow 0 = 2b - a = 0 \rightarrow a = 0 \quad (2.25)$$

$$\pi_3 = U_m^{\ 0} \rho^0 B^{-1} d_{50}^{\ 1} = \frac{d50}{B} \quad (2.26)$$

$$\pi_4 = U_m^{\ a} \rho^b B^c S^1 \quad (2.27)$$

$$K^0 L^0 T^0 = (LT^{-1})^a (KL^{-4}T^2)^b L^c (L)^1 \quad (2.28)$$

$$K \rightarrow 0 = b \ \rightarrow b = 0 \quad (2.29)$$

$$L \rightarrow 0 = a - 4b + c + 1 \rightarrow c = -1 \quad (2.30)$$

$$T \rightarrow 0 = 2b - a = 0 \rightarrow a = 0 \quad (2.31)$$

$$\pi_4 = U_m^{\ 0} \rho^0 B^{-1} S^1 = \frac{S}{B} \quad (2.32)$$

$$\pi_5 = U_m^{\ a} \rho^b B^c \rho_s^{\ 1} \quad (2.33)$$

$$K^0 L^0 T^0 = (LT^{-1})^a (KL^{-4}T^2)^b L^c (KL^{-4}T^2)^1 \quad (2.34)$$

$$K \rightarrow 0 = b + 1 \rightarrow b = -1 \tag{2.35}$$

$$L \rightarrow 0 = a - 4b + c - 4 \rightarrow c = 0 \tag{2.36}$$

$$T \rightarrow 0 = 2b - a + 2 \rightarrow a = 0 \tag{2.37}$$

$$\pi_5 = U_m^{\,0} \rho^{-1} B^0 \rho_s^{\,1} = \frac{\rho_s}{\rho} \tag{2.38}$$

$$\pi_6 = U_m^{\,a} \rho^b B^c L^1 \tag{2.39}$$

$$K^0 L^0 T^0 = (LT^{-1})^a (KL^{-4}T^2)^b L^c L^1 \tag{2.40}$$

$$K \rightarrow 0 = b \rightarrow b = 0 \tag{2.41}$$

$$L \rightarrow 0 = a - 4b + c + 1 \rightarrow c = -1 \tag{2.42}$$

$$T \rightarrow 0 = 2b - a \rightarrow a = 0 \tag{2.43}$$

$$\pi_6 = U_m^{\,0} \rho^0 B^{-1} L^1 = \frac{L}{B} \tag{2.44}$$

$$\pi_7 = U_m^{\,a} \rho^b B^c g^1 \tag{2.45}$$

$$K^0 L^0 T^0 = (LT^{-1})^a (KL^{-4}T^2)^b L^c (LT^{-2})^1 \tag{2.46}$$

$$K \rightarrow 0 = b \rightarrow b = 0 \tag{2.47}$$

$$L \rightarrow 0 = a - 4b + c + 1 \rightarrow c = +1 \tag{2.48}$$

$$T \rightarrow 0 = 2b - a - 2 \rightarrow a = -2 \tag{2.49}$$

$$\pi_7 = U_m^{\,-2} \rho^0 B^1 g^1 = \frac{B * g}{Um^2} = Fr^{\,-2} \tag{2.50}$$

$$\pi_8 = U_m^{\,a} \rho^b B^c H^1 \tag{2.51}$$

$$K^0 L^0 T^0 = (LT^{-1})^a (KL^{-4}T^2)^b L^c L^1 \tag{2.52}$$

$$K \rightarrow 0 = b \rightarrow b = 0 \qquad (2.53)$$

$$L \rightarrow 0 = a - 4b + c + 1 \rightarrow c = -1 \qquad (2.54)$$

$$T \rightarrow 0 = 2b - a \rightarrow a = 0 \qquad (2.55)$$

$$\pi_8 = U_m^{\,0} \rho^0 B^{-1} H^1 = \frac{H}{B} \qquad (2.56)$$

$$\pi_9 = U_m^{\,a} \rho^b B^c h^1 \qquad (2.57)$$

$$K^0 L^0 T^0 = (LT^{-1})^a (KL^{-4}T^2)^b L^c L^1 \qquad (2.58)$$

$$K \rightarrow 0 = b \rightarrow b = 0 \qquad (2.59)$$

$$L \rightarrow 0 = a - 4b + c + 1 \rightarrow c = -1 \qquad (2.60)$$

$$T \rightarrow 0 = 2b - a \rightarrow a = 0 \qquad (2.61)$$

$$\pi_9 = U_m^{\,0} \rho^0 B^{-1} h^1 = \frac{h}{B} \qquad (2.62)$$

If the dimensional analysis is repeated with the Buckingham-π theorem by choosing the repeated dimensional quantities U_m, ρ and H:

$$\pi_{10} = U_m{}^a \rho^b H^c g^1 = (LT^{-1})^a (KL^{-4}T^2)^b (L)^c (LT^{-2})^1 = K^0 L^0 T^0 \qquad (2.63)$$

$$\text{K için } 0 = b \qquad (2.64)$$

$$\text{T için } 0 = -a + 2b - 2 \qquad a=-2 \qquad (2.65)$$

$$\text{L için } 0 = a - 4b + c + 1 \qquad c=1 \qquad (2.66)$$

$$\pi_{10} = \frac{H\,g}{U_m{}^2} = Fr^{-2} \qquad (2.67)$$

$$\pi_{11} = U_m{}^a \rho^b H^c T^1 = (LT^{-1})^a (KL^{-4}T^2)^b (L)^c (T)^1 = K^0 L^0 T^0 \qquad (2.68)$$

$$\text{K için } 0 = \text{b} \tag{2.69}$$

$$\text{T için } 0 = -\text{a} + 2\text{b} + 1 \quad \text{a=1} \tag{2.70}$$

$$\text{L için } 0 = \text{a} - 4\text{b} + \text{c} \quad \text{c=-1} \tag{2.71}$$

$$\pi_{11} = \frac{\text{U}_\text{m}\,\text{T}}{\text{H}} = KC \tag{2.72}$$

$$\pi_{12} = \text{U}_\text{m}{}^{\text{a}}\rho^{\text{b}}\text{H}^{\text{c}}\text{h}^{1} = (\text{LT}^{-1})^{\text{a}}(\text{KL}^{-4}\text{T}^{2})^{\text{b}}(\text{L})^{\text{c}}(\text{L})^{1}\text{=K}^{0}\text{L}^{0}\text{T}^{0} \tag{2.73}$$

$$\text{K için } 0 = \text{b} \tag{2.74}$$

$$\text{T için } 0 = -\text{a} + 2\text{b} \quad \text{a=0} \tag{2.75}$$

$$\text{L için } 0 = \text{a} - 4\text{b} + \text{c} + 1 \quad \text{c=}-1 \tag{2.76}$$

$$\pi_{12} = \frac{\text{h}}{\text{H}} \tag{2.77}$$

$$\pi_{13} = \text{U}_\text{m}{}^{\text{a}}\rho^{\text{b}}\text{H}^{\text{c}}\text{L}^{1} = (\text{LT}^{-1})^{\text{a}}(\text{KL}^{-4}\text{T}^{2})^{\text{b}}(\text{L})^{\text{c}}(\text{L})^{1}\text{=K}^{0}\text{L}^{0}\text{T}^{0} \tag{2.78}$$

$$\text{K için } 0 = \text{b} \tag{2.79}$$

$$\text{T için } 0 = -\text{a} + 2\text{b} \quad \text{a=0} \tag{2.80}$$

$$\text{L için } 0 = \text{a} - 4\text{b} + \text{c} + 1 \quad \text{c=}-1 \tag{2.81}$$

$$\pi_{13} = \frac{\text{L}}{\text{H}} \tag{2.82}$$

$$\pi_{14} = \text{U}_\text{m}{}^{\text{a}}\rho^{\text{b}}\text{h}^{\text{c}}\mu^{1} = (\text{LT}^{-1})^{\text{a}}(\text{KL}^{-4}\text{T}^{2})^{\text{b}}(\text{L})^{\text{c}}(\text{KL}^{-2}\text{T})^{1}\text{=K}^{0}\text{L}^{0}\text{T}^{0} \tag{2.83}$$

$$\text{K için } 0 = \text{b} + 1 \quad \text{b} = -1 \tag{2.84}$$

$$\text{T için } 0 = -\text{a} + 2\text{b} + 1 \quad \text{a=}-1 \tag{2.85}$$

$$\text{L için } 0 = \text{a} - 4\text{b} + \text{c} - 2 \quad \text{c=}-1 \tag{2.86}$$

$$\pi_{14} = \frac{\mu}{H\,\rho\,U_m} = Re^{-1} \tag{2.87}$$

$$\pi_{15} = U_m{}^a \rho^b H^c \rho_s{}^1 = (LT^{-1})^a (KL^{-4}T^2)^b (L)^c (KL^{-4}T^2)^1 = K^0L^0T^0 \tag{2.88}$$

$$K \text{ için } 0 = b + 1 \qquad b=-1 \tag{2.89}$$

$$T \text{ için } 0 = -a + 2b + 2 \qquad a=0 \tag{2.90}$$

$$L \text{ için } 0 = a - 4b + c - 4 \quad c=0 \tag{2.91}$$

$$\pi_{15} = \frac{\rho_s}{\rho} = G_s \tag{2.92}$$

$$\pi_{16} = U_m{}^a \rho^b H^c d_{50}{}^1 = (LT^{-1})^a (KT^{-4}T^2)^b (L)^c (L)^1 = K^0L^0T^0 \tag{2.93}$$

$$K \text{ için } 0 = b \tag{2.94}$$

$$T \text{ için } 0 = -a + 2b \qquad a=0 \tag{2.95}$$

$$L \text{ için } 0 = a - 4b + c + 1 \quad c=-1 \tag{2.96}$$

$$\pi_{16} = \frac{d_{50}}{H} \tag{2.97}$$

$$\pi_{17} = U_m{}^a \rho^b H^c S^1 = (LT^{-1})^a (KT^{-4}T^2)^b (L)^c (L)^1 = K^0L^0T^0 \tag{2.98}$$

$$K \text{ için } 0 = b \tag{2.99}$$

$$T \text{ için } 0 = -a + 2b \qquad a=0 \tag{2.100}$$

$$L \text{ için } 0 = a - 4b + c + 1 \quad c=-1 \tag{2.101}$$

$$\pi_{17} = \frac{S}{H} \tag{2.102}$$

Apart from the dimensionless parameters listed above, there are some effective dimensionless numbers in the literature such as Shields parameter (2.2), dimensionless time scale (3.6), grain Froude number (2.103), Iribarren number (2.104), relative grain median diameter (2.105).

$$Fr_d = \frac{U_m}{\sqrt{(g(s-1)d_{50})}} \tag{2.103}$$

$$\mathrm{Ir} = \frac{tan\alpha}{\sqrt{\frac{H}{L_0}}} \tag{2.104}$$

$$\frac{\mathrm{L}}{\mathrm{d}_{50}} \tag{2.105}$$

As a conclusion, it was obtained the functional relation given by equations 2.106 and 2.107. As can be seen, the number of effective dimensionless parameters is quite high in a physical event where local ground movements are examined in the head section. The dimensionless parameters affecting the scour under the steady streaming effect is given in equation 2.106, while in case of plunging breaker effect they vary as shown in equation 2.107.

$$\frac{s}{B} = f(Re_D, KC, \frac{d_{50}}{B}, Fr, \frac{h}{B}, \frac{H}{B}, \frac{L}{B}, \frac{S}{B}, \frac{\rho_S}{\rho}, \Theta, Fr_d, Ir, \frac{\mathrm{L}}{\mathrm{d}_{50}} ...) \tag{2.106}$$

$$\frac{s}{H} = f(Re_D, KC, \frac{d_{50}}{H}, Fr, \frac{h}{H}, \frac{H}{B}, \frac{L}{H}, \frac{S}{H}, \frac{\rho_S}{\rho}, \Theta, Fr_d, Ir, \frac{\mathrm{L}}{\mathrm{d}_{50}} ...) \tag{2.107}$$

CHAPTER THREE
LITERATURE REVIEW

Researchers have carried out some experimental studies to comprehend formation of scour. In the literature, researchers have examined the scour for the trunk and head section. In this section, previous studies are examined under three different headings: head section, trunk section and mode of sediment transport.

3.1 Head Section

Studies on the head section of the breakwater are very limited compared to the trunk section. The studies carried out in the literature are also performed for the non-breaking wave case. There are no any studies in the head section for the breaking wave case. This thesis is important because it fills the gap in the literature.

There are two types of scour: the scour around the trunk and the head section. For the scour in the trunk section, if the waves affect the trunk of the breakwater at an angle of 90 degrees, two-dimensional scour occurs in the trunk section. However, this situation does not occur in any way in the head section. Three-dimensional scour always occurs in the head section.

Fredsøe and Sumer (1997, 2000) researched the scour in the head section. Consequently, they concluded that the scour in the head section can be of great value as a result of these studies. In addition, they confirmed the results reported by Lillycrop and Hughes (1993). Therefore, the investigation of the local scour in the head section of the breakwaters has great importance.

The scour mechanism in the head and trunk section of breakwaters differs. Unlike the trunk section, 3-D scour is always seen in the head section. There is also a difference in the definition of the *KC* number in the head section. It is defined according to the base width of the breakwater. The formula of the *KC* can be seen in equation 2.7. In addition, Fredsøe and Sumer (1997) stated that unlike the trunk section, scour caused by the plunging breaker mechanism occurs in addition to the scour caused by the steady streaming mechanism.

In their study, Fredsøe and Sumer (1997) experimentally examined the local scour in the head section of a rubble-mound breakwater for regular and irregular wave conditions. They showed that two main mechanisms are causing the local scour in the head section. The first mechanism is the local scour induced by steady streaming. This mechanism leads to a scour area on the side where the waves approach the breakwater (Area M in Fig. 3.1). The other is the local scour caused by plunging breaker (Area P in Fig. 3.1). This occurs when waves are big enough to climb over the breakwater, and plunging breaker may take place on the lee-side of the breakwater. It forms as a consequence of waves which has a sufficient height, climbing over the breakwater. In addition, N and Q correspond to depositon areas in the figure below. The scour areas caused by the mechanisms mentioned above can be seen in Fig. 3.1.

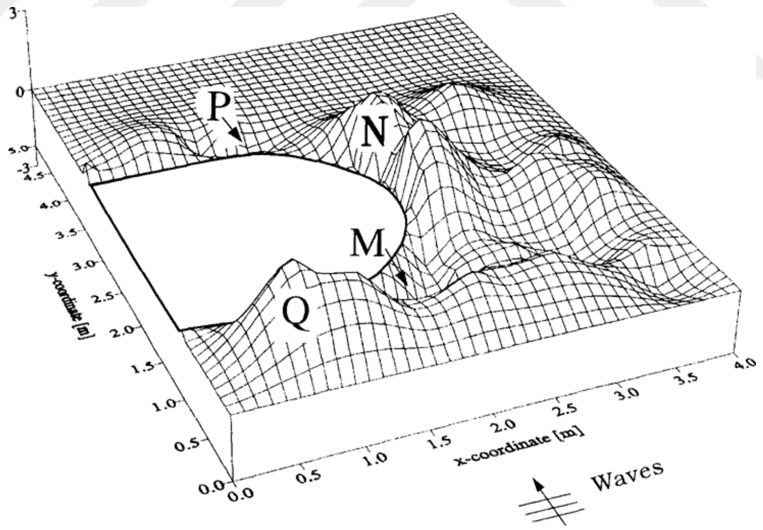

Figure 3.1 Bed topography around the head section (Fredsøe and Sumer, 1997)

According to their study, the main mechanism that causes scour caused by steady streaming in the head section is lee-wake vortices. Sediment particles exposed to these vortices eventually pile up away from the breakwater head section, causing a clear scour in the breakwater head section. In addition to that, they stated that the main parameter that causes lee-wake vortices is Keulagen Karpenter number, *KC*. It means that the scour in the head section is governed by this number. The higher the number *KC*, the greater is the scour.

For the case of scour caused by steady streaming, the scour relates to the following quantities: U_m, T_w, B, the bed roughness, d, the kinematic viscosity, v, and the side slope of the breakwater, m. It means the relative maximum scour depth is the function of the quantities below:

$$\frac{S}{B} = f(KC, \theta, m\,, a/d, RE) \tag{3.1}$$

However, in the live-bed conditions ($\theta > \theta_{cr}$), the scour and deposition characteristics only vary with *KC* number. The relative maximum scour depth caused by steady streaming as follows:

$$\frac{S}{B} = 0.04C_1[1 - \exp(-4(\mathrm{KC} - 0.05))] \tag{3.2}$$

where C_1 is the uncertainty factor with a mean value of 1 and its standard deviation is 0.2.

Equation (3.2) is valid for streaming-caused scour, and plunging-breaker-caused scour depends on different parameters. The scour can be obtained to correlate with the non-dimensional parameters as below:

$$\frac{\mathrm{S}}{\mathrm{H_s}} = \mathrm{f}\left(\frac{\mathrm{T_p}\sqrt{\mathrm{gH_s}}}{\mathrm{h}}, \theta, \mathrm{m}\right) \tag{3.3}$$

where

H_S: significant wave height

T_p: peak wave period

g: acceleration due to gravity

In the live-bed conditions when $\theta > \theta_{cr}$, the plunging-breaker-induced scour will only vary with the non-dimensional parameter of $T_p\sqrt{gH_s}/h$. The numerator, $T_p\sqrt{gH_s}$, physically represents the amount of water penetrating into the main body of the water as a result of plunging breaker. In addition, the experimental results from studies of Lillycrop and Hughes (1993) can be seen in Figure 3.2. It demonstrates that there is a significant relation between the studies of Fredsøe and Sumer (1997) and Lillycrop and Hughes (1993).

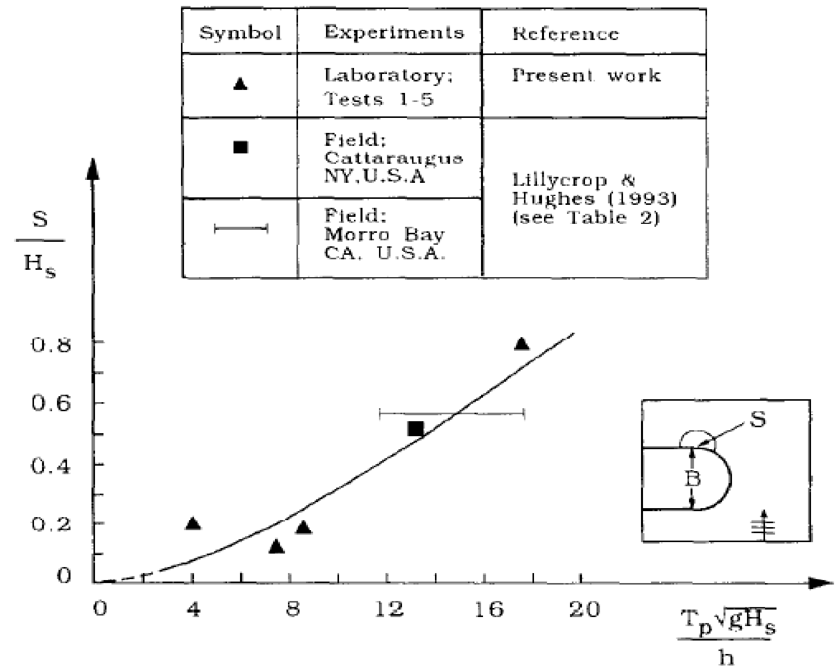

Figure 3.2 Maximum scour depths caused by plunging breaker. Live bed. Sumer and Fredsøe (2002)

As a result, Sumer and Fredsøe (2002) concluded that the scour depth caused by plunging breaker can be obtained as a result of the experiment as follows:

$$\frac{S}{H_s} = 0.01C_2 \left(\frac{T_p\sqrt{gH_s}}{h}\right)^{1.5} \tag{3.4}$$

where C_2 is an uncertainty factor with a mean value of 1 and its standard deviation is 0.34.

Plunging breaker can occur when the waves are large enough to exceed the breakwater head as demonstrated in Figure 3.3. Braker's evolution over time can be seen in the figure. This evolution has been achieved as a result of a video recording. An underwater camera was used to monitor this process underwater by the way. Here, the breaker is three-dimensional and creates a jet that will cause scour. As shown in Fig. 3.3, the jet hits the bed (Frame 3) and mobilizes the sediments particles (Frame 4). The scour caused by the plunging breaker corresponds to Area P as mentioned in Fig. 3.1. On the other side, to examine the effect of the plunging breaker on scour, a vertical plate was placed from the top of the breakwater to its bottom (The aim is to prevent the formation of plunging breaker). As a consequence of this test, it was noticed that no scour took place at this location. The conclusion here is that scour is only caused by the plunging breaker at this location (Area P).

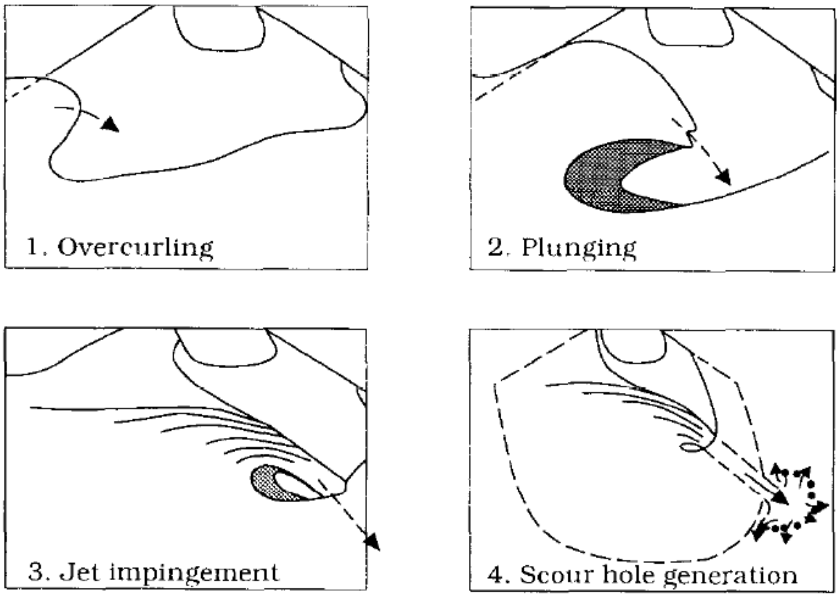

Figure 3.3 Time evolution of plunging breaker on the breakwater head (Fredsøe and Sumer, 1997)

Burcharth and Liu (1995) did a work related to the failure modes of a rubble-mound breakwater. For breakwater structures, where any demolition can cause significant cost increases, this study is important for breakwater designers in terms of showing the failure modes. In this way, the designers will be able to take precautions against any damage may occur in the breakwaters. Fig. 3.4 shows the situations that may disrupt stability of breakwaters. As can be seen in the figure, there are many failure modes such as: slip failure, erosion, breakage of armour, subsoil settlement, etc. At this point, the strength of the soil on which the breakwater is positioned directly affects the stability of the structure. Scour causes damage to the structure by disrupting its stability of the structure.

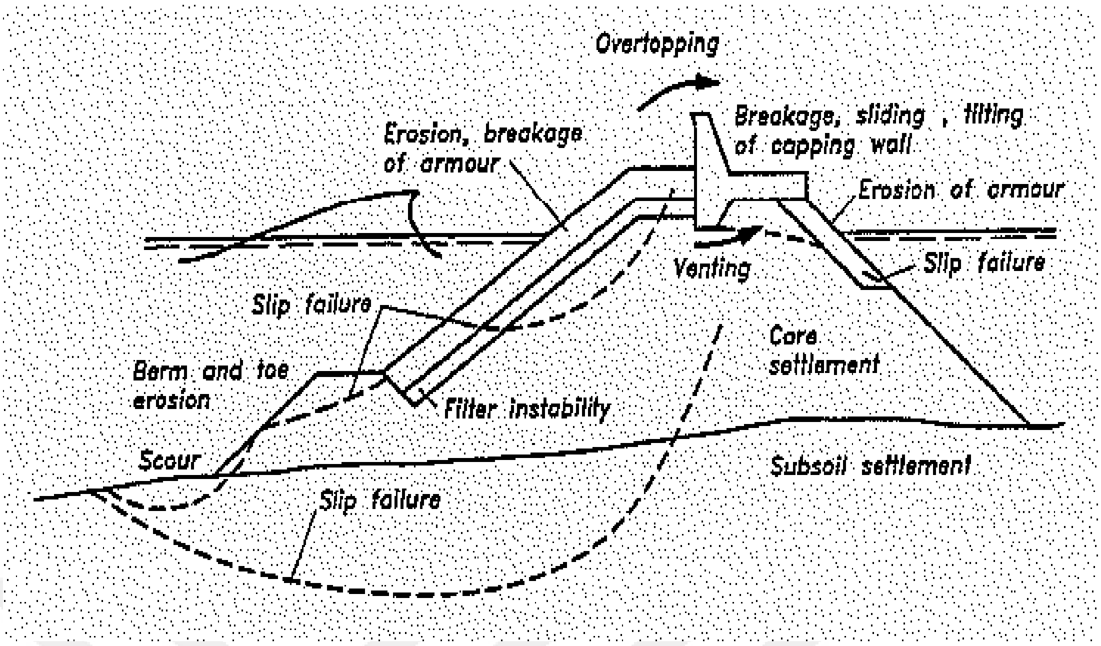

Figure 3.4 Situations that may cause the destruction of a rubble-mound breakwater (Burcharth, 1993)

Myrhaug, Rue, and Tørum (2004) revealed the difference between their study and the study of Fredsøe and Sumer (1997). It was observed that the results of scour depth and protective layer thickness seen on the head section were slightly smaller than the results from waves with the highest one-third wave height (H_s) according to Sumer and Fredsøe.

There are also studies in which scour formation is researched both experimentally and numerically. In their study, Temel and Dogan (2021) compared the experimental and numerical results of the scour being formed at the rubble-mound breakwater trunk. It is interpreted that there is a good harmony between the numerical model and the experimental results. Gislason, Fredsøe, and Sumer (2009) who investigated the scour experimentally and numerically stated that the results were compatible for the vertical-wall breakwater, but they could not reach a satisfactory result for the sloping-wall breakwater.

As a result of their experimental study, Fredsøe and Sumer (1997) expressed the time-dependent variation of scour and deposition as shown in Fig. 3.5. As given in the figure, part number one corresponds to the steady streaming induced scour region, while part number two corresponds to deposition region. The areas of scour and deposition in the head section were mentioned in detail above (Fig. 3.1). As mentioned in the "Mechanics of Scour" section, the scour occurs in two different stages as scour development and equilibrium stage. Fig. 3.6 displays the time-dependent variation of scour caused by the plunging breaker on the lee side (Area P in Fig. 3.1). As given in Fig. 3.5 and 3.6, scour due to steady streaming reaches its final value at approximately 3 cm, while scour due to plunging breaker reaches its final value at approximately 2 cm.

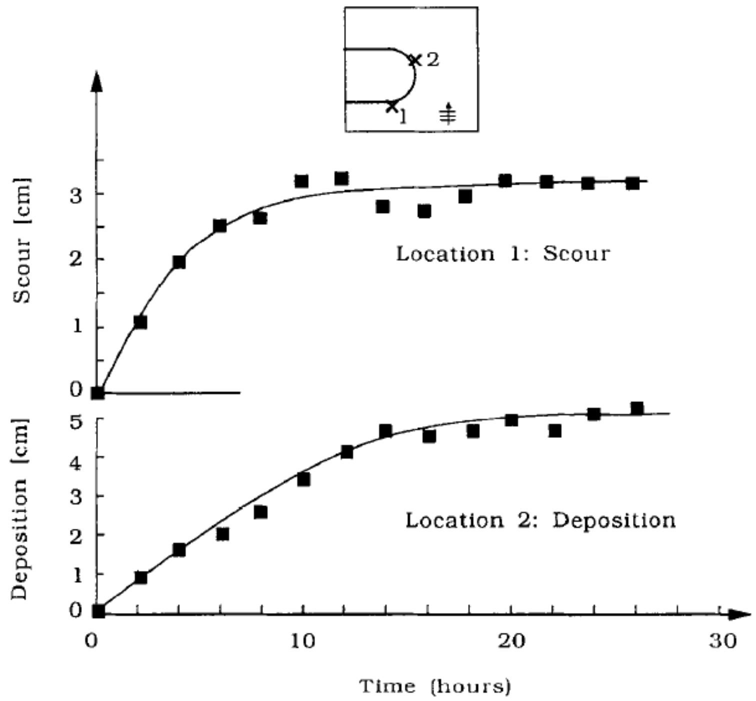

Figure 3.5 Change in scour and depostion depths with time caused by steady streaming (Fredsøe and Sumer, 1997)

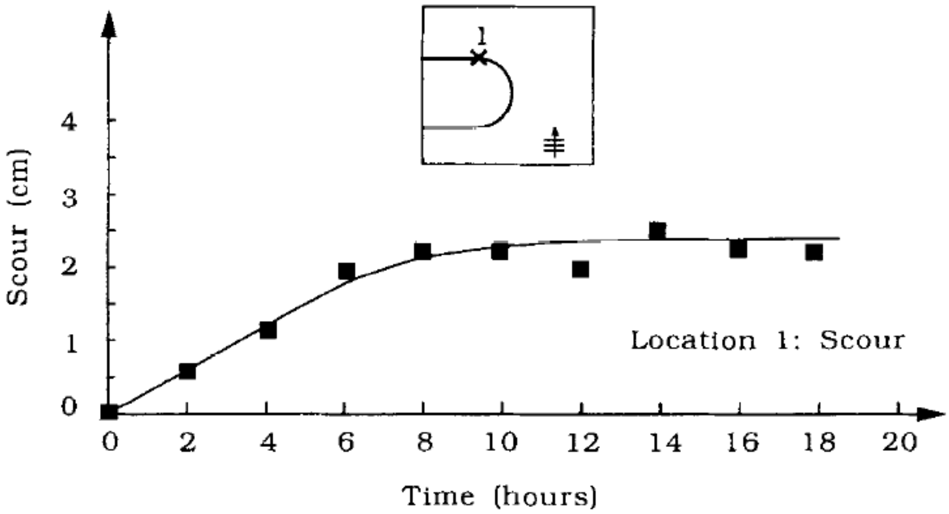

Figure 3.6 Change in scour and deposition depths with time caused by plunging breaker (Fredsøe and Sumer, 1997)

Fredsøe and Sumer (1997) studied the variation of lee-wake vortices that cause scour induced by steady streaming (Fig. 3.7). As mentioned earlier, the larger the lee-wake vortices, the larger the scour. In the figure, the L_x notation indicates the length of the lee-wake vortices in x direction. L_y notation indicates the length of the lee-wake vortices in y direction. As seen in the figure below, lee-wake vortices do not form until the KC value reaches one. Furthermore, the effect of side slope is sensed after the *KC* number arrives at two. The conclusion is that side slope reduces the dimensions of the lee-wake vortices and as a result, the scour in the head section is reduced.

The KC value is always less than one due to the dimensions of breakwaters in real-life situation. So, this means that the lee-wake vortices have no effect on the scour for the real case.

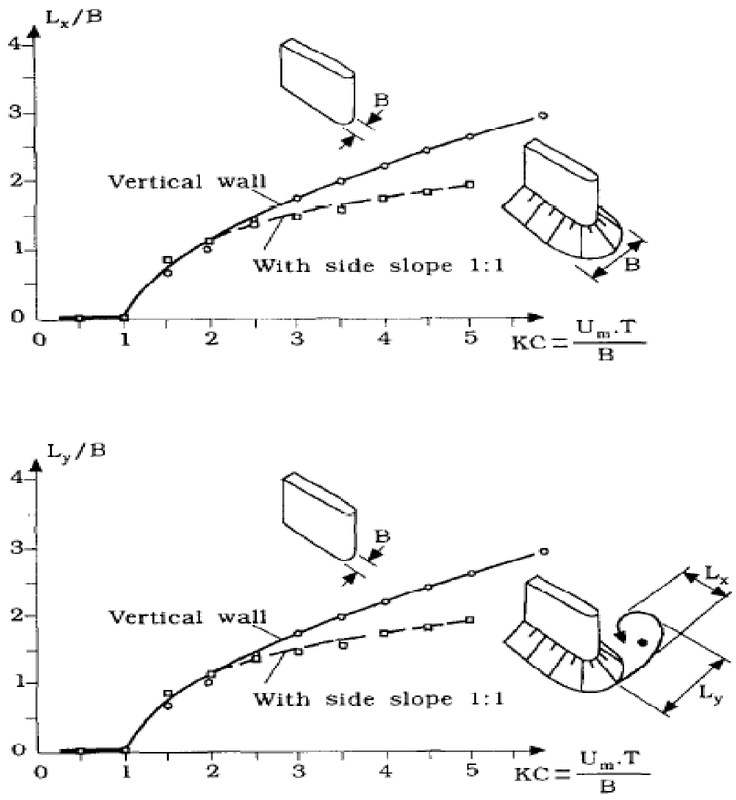

Figure 3.7 Variation of lee-wake vortices with respect to the KC number (Fredsøe and Sumer, 1997)

The dimensions of the lee-wake vortices are analyzed by areas (Area M, N and P) in Fig. 3.8. The dimensions of the areas were nondimensionalized with *B* as in Fig. 3.7. The areas under the influence of steady streaming are sketched as a function of the KC number (Fig. 3.8a-b), while the area under the influence of the plunging breaker is plotted as a function of $T_p\sqrt{gH_s}$ / h (Fig. 3.8c). The results obtained from Fig. 3.8 are presented below, respectively.

First, the scour area induced by steady-streaming (Area M) is wider than the deposition area (Area N). Because, the scoured sediment particles in Area M move to the Area N, Q and R as explained ealier (Fig. 3.1).

Second, in Figure 3.8a, as the KC number increases, scour increases, while in Figure 3.8b, a strong direct relationship cannot be established between the KC number and deposition. This situation might be related to the geometry of the part where the deposition region is located.

Third, the scour area (Area P) caused by the plunging breaker does not depend on the parameter $T_p\sqrt{gH_s}$ / h. Despite the period increased significantly, no significant change was observed in the nondimensionalized lee-wake vortices.

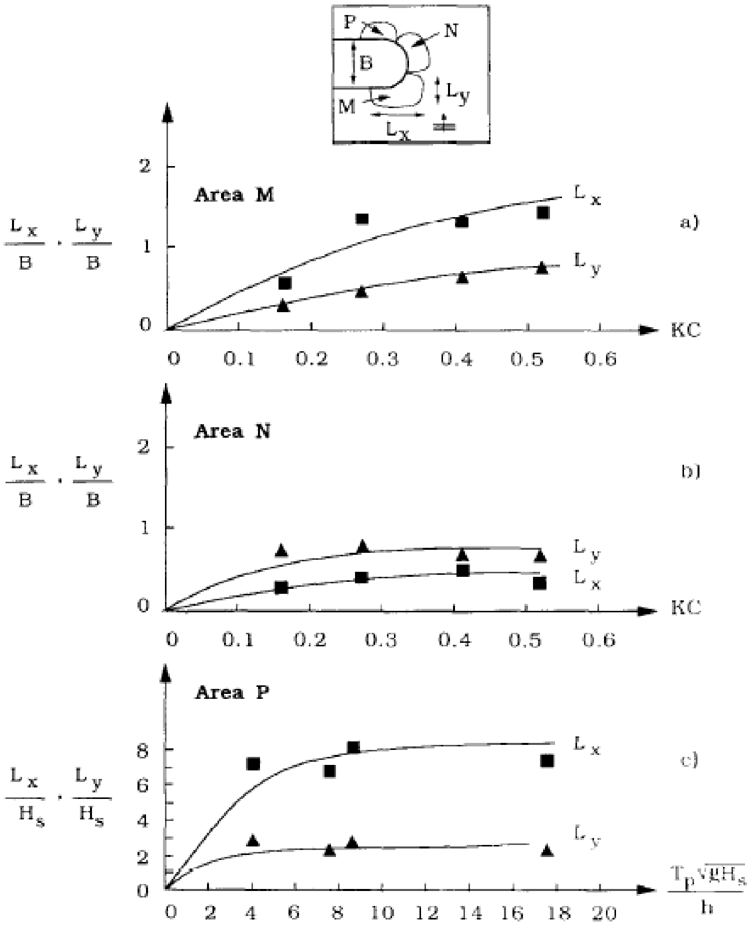

Figure 3.8 Dimension of scour/deposition areas in breakwater head (Fredsøe and Sumer, 1997)

Fig. 3.9 demostrates location of maximum scour and deposition points in the head section. In the figure, the rounded dots represent the maximum scour and deposition depth points under the steady streaming effect, while the triangular symbol shows the scour caused by plunging breaker. While the location of the maximum scour depth moves to the offshore direction in Figure 3.9a, the location of the maximum deposition depth moves to the shoreside in Figure 3.9b. It means the locations of maximum scour and deposition depth moves in opposite directions. This situation is due to the KC number and increase in streaming area.

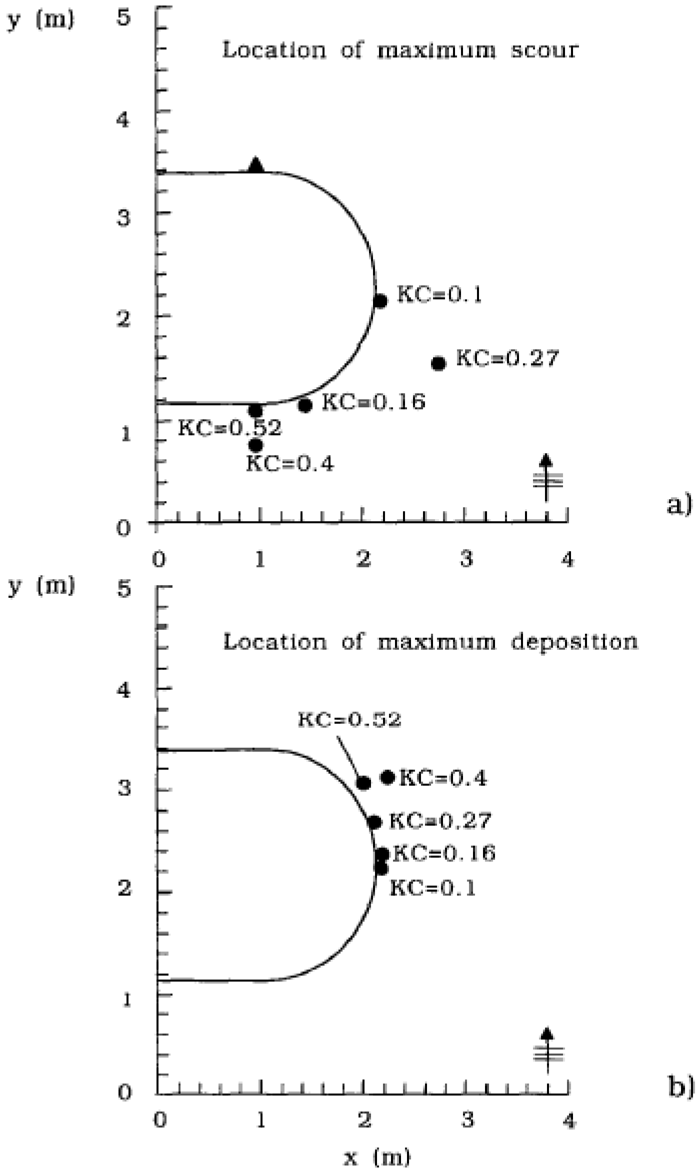

Figure 3.9 Positions of maximum scour and deposition depth in breakwater head (Fredsøe and Sumer, 1997)

As a conlusion, Fredsøe and Sumer (1997) examined the scour that may occur in the rubble-mound breakwater head and reached the following conclusions:

- There are two situations that cause scour: steady streaming and plunging breaker.
- The head scour is controlled by the Keulagen Karpenter number, *KC*. As the *KC* value goes up, the scour also goes up.
- Steady streaming can cause not only scour, but also deposition.
- A protective layer can be built to prevent scour formation. The dimensions (width and number of layers) required for the design of the protective layer will be given in section 3.2.
- For the steady streaming case, the *KC* number is the essential parameter affecting the scour depending on the base width of the breakwater head, while for the plunging breaker case, wave period, wave height, water depth and gravitational acceleration are the main parameters affecting the scour. As these parameters increase, the scour depth increases.

3.2 Trunk Section

The reason for the formation of the scour in front of any coastal structure is the disruption of the steady streaming. The presence of the structure changes the flow structure and causes the scour. Thus, the amplification factor, *a*, will increase around the structure and the scour will decrease as the amplification factor decreases as it moves away from the structure.

For a vertical-wall breakwater, the incident wave hits the breakwater with a 90-degree surface inclination and is reflected back to the offshore direction. Thus, when the incident wave and the reflected wave are superposed, a standing wave is occured Dean and Dalrymple (1984). Carter, Liu, and Mei (1973) were the first to notice the scour and deposition process caused by the standing waves. Figure 3.18 demonstrates the occurrence of the standing waves. For rubble-mound breakwaters, since the surface slope is smaller, the reflection coefficient is smaller. Additively, the construction material is stone which means some energy of the incident waves are absorbed. For the no-suspension case, Sumer and Fredsøe (2000) concluded that the maximum scour depth decreases as the surface slope angle decreases. As can be seen in Figure 3.10

below, there is a big reduction in the maximum scour depth. While it reaches the order of 0.9 for α = 90°, it reaches 0.3 for α = 30°.

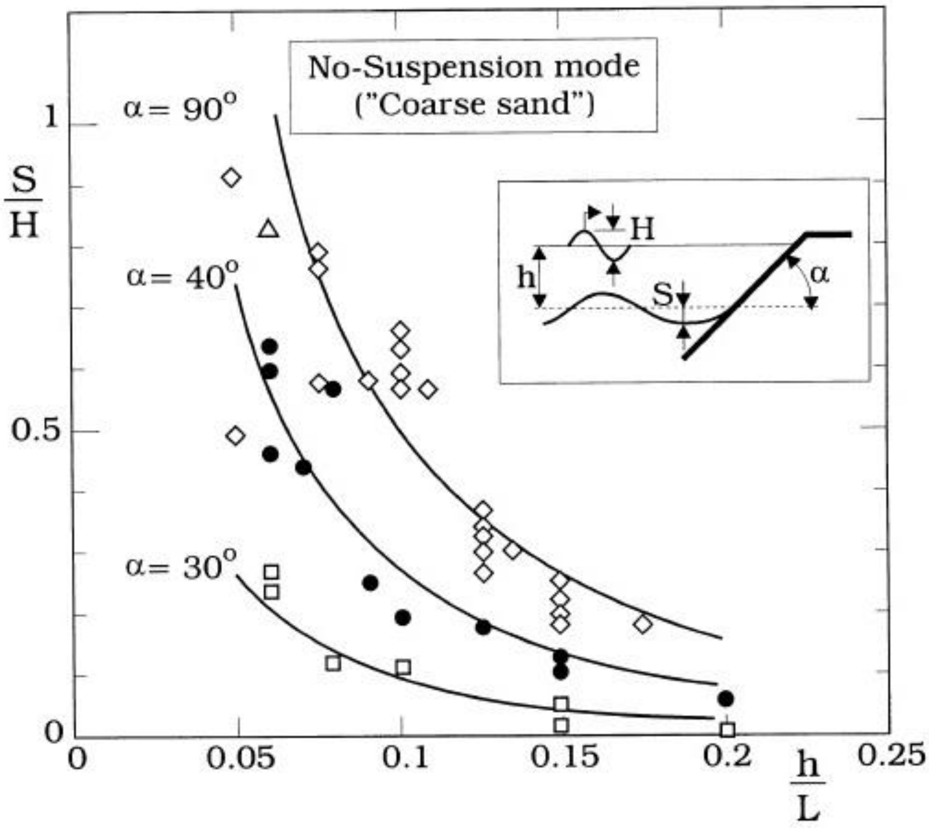

Figure 3.10 Maximum scour depths (Sumer and Fredsøe, 2000)

The empirical expression of Figure 3.10 is given as below:

$$\frac{S}{H} = \frac{f(\alpha)}{\sinh\left(\frac{2\pi h}{L}\right)^{1.35}} \quad ; \quad f(a) = 0.3 - 1.77\exp\left(-\frac{a}{15}\right) \qquad (3.5)$$

where h, water depth, H, incident wave height, L, incident-wave length, and a is the surface slope of the breakwater in the range 30° ≤ a ≤ 90°. Equation 3.5 gives the relative scour depth in the trunk section. This study was carried out for regular wave and d_{50} = 0.2 mm. The study of Sumer and Fredsøe (2000) showed a good harmony with the numerical results of Arneborg, Hansen and Juhl (1995 a and b).

In the scour studies, not only the equilibrium scour depth, but also the time necessary for scour to arrive at its equilibrium state (time scale, *T*) is investigated. The time scale parameter, *T*, is nondimensionalized and expressed with the symbol T^* as follows according to Sumer and Fredsøe (2000):

$$T^* = \frac{\left(g(s-1)d_{50}^3\right)^{\frac{1}{2}}}{H^2}T \tag{3.6}$$

Figure 3.11 shows the time-dependent changes of the scour as a result of Sumer and Fredsøe 's study (2000). In Fig. 3.11, time scale parameters are obtained by drawing the tangents to the curves. Then, with the help of equation 3.6, the time scale is nondimensionalized, that is, normalized. From Fig. 3.11, the equilibrium scour depth, which was 4.8 cm in case of the regular wave case, decreased to 2.2 cm in case of the irregular wave case.

Table 3.1 shows the change of time scale according to *h*/*L*. The time scale was nondimensionalized with the help of equation 3.6 and the nondimensionalized time scale parameter, T^*, was obtained. In Table 3.1, there is an inverse relationship between *h*/*L* and T^* parameters. As *h*/*L* decreases, T^* increases.

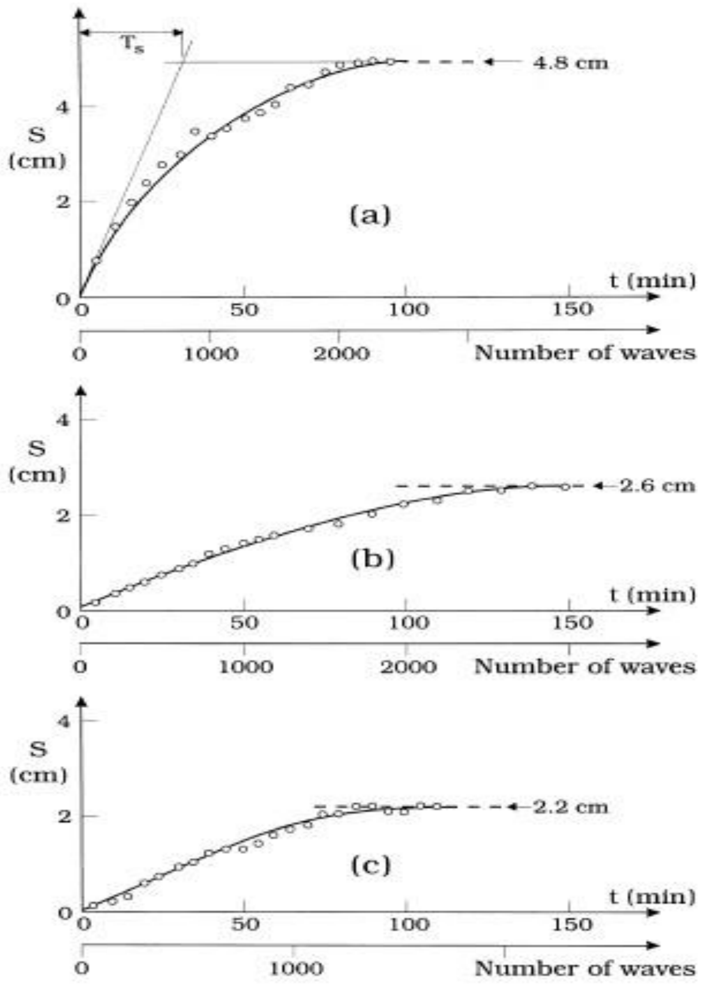

Figure 3.11 Time development of scour (Sumer and Fredsøe, 2000)

Table 3.1 Time scale of scour

Case	Slope	Wave type	h/L	Time scale, T (min)	Number of waves corresponding to T	Normalized time scale (T^*)
a	1:1.2	Regular	0.078	33	800	3.3
b	1:1.7	Regular	0.06	85	1700	6
c	1:1.2	Irregular	0.045	78	1200	15.8

The breakwater model used by Sumer and Fredsøe (2000) is presented in Fig. 3.12. Two different breakwater models were prepared. The breakwater is in contact with the channel bottom in Fig. 3.13a while the breakwater rests on the sandy floor in Fig. 3.13b. For this reason, Fig. 3.13a has more structural stability than Fig. 3.13b. This means stone material used in the construction of the breakwater will not easily fall into the scour hole and fill it (Fig. 3.13a). On the contrary, if the breakwater sits on sandy ground (Fig. 3.13b), stones may fill the scour hole, resulting in a reduction in scour depth. This situation reflects the real-life situation (Fig.3.13b). Sumer and Fredsøe (2000) obtained that scour reduced by about 30% if the breakwater was set on sandy floor instead of the channel bottom (Fig. 3.14). In addition, penetration of the flow into the breakwater is another condition that affects the scour. If the breakwater rests on a sandy ground (Fig.3.13b), the flow through the breakwater will be less, so the scour will be less.

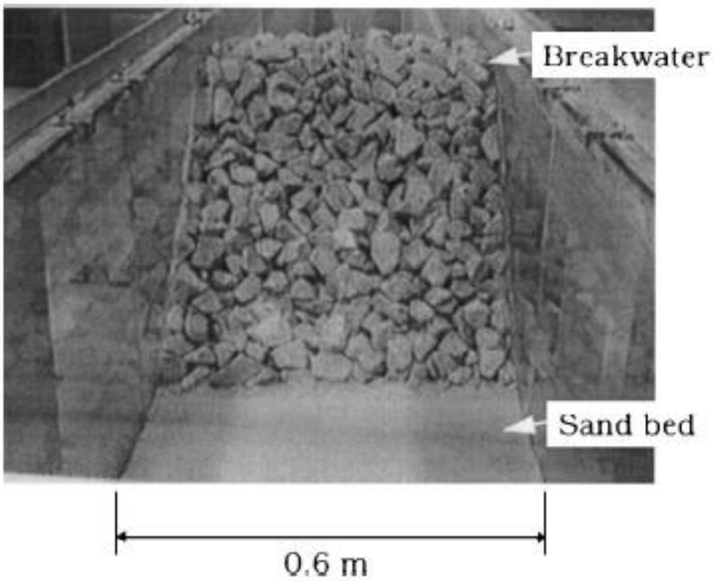

Figure 3.12 The image of breakwater model of Sumer and Fredsøe (2000). Slope 1:1.75

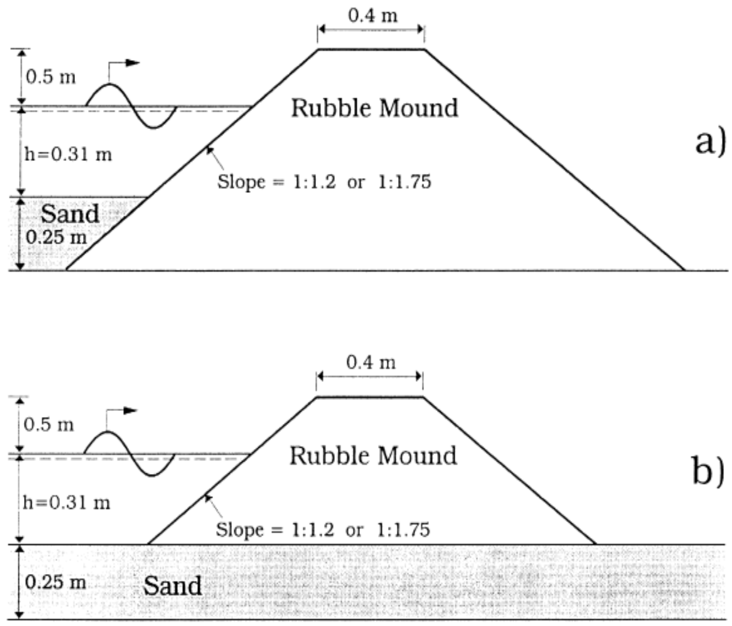

Figure 3.13 Cross-section of the breakwater in Sumer and Fredsøe 's experimental study (2000)

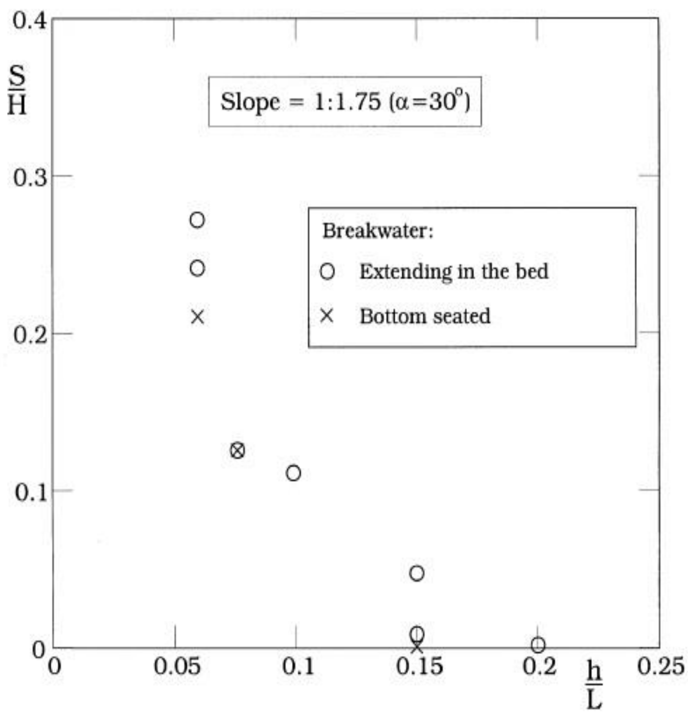

Figure 3.14 Maximum scour depths obtained in front of the breakwater model on the sand and channel floor (Sumer and Fredsøe, 2000)

The maximum scour depths seen in regular and irregular wave states are given in Figure 3.15. The maximum scour in case of irregular waves was reduced by a factor of two for slope 1:1.2 as can be seen in Fig. 3.15. Another conclusion is the quantitative compatibility between the study of Hughes and Fowler (1991) and the study of Sumer and Fredsøe (2000) for the case of vertical-wall breakwater.

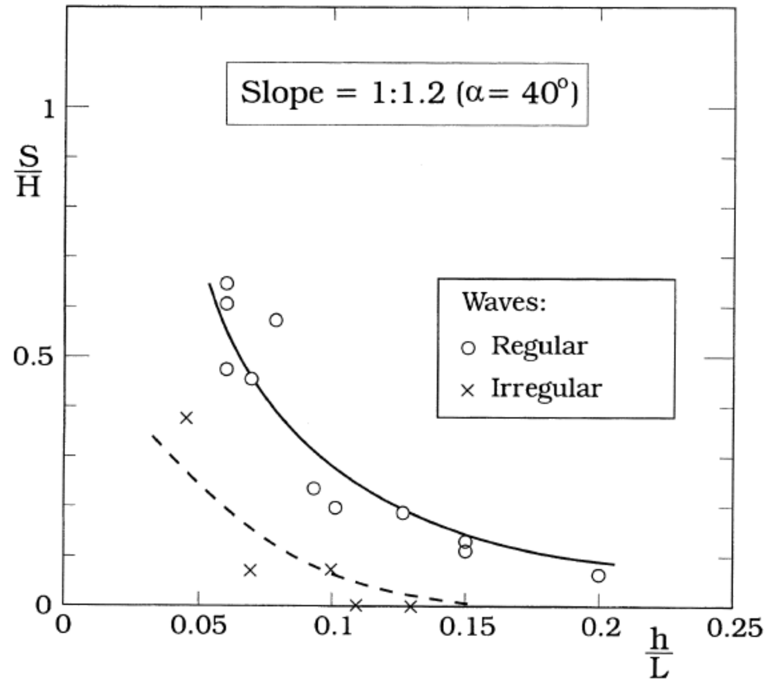

Figure 3.15 Maximum scour depths in case of regular and irregular wave cases (Sumer and Fredsøe, 2000)

Scour/Deposition may occur basically by the effect of current and wave around breakwaters. The pattern of the scour/deposition changes due to the geometry of the structure, characteristics of the waves, median grain diameter of the seabed material, wave breaking condition, etc. Scour studies are important for the long life of the rubble-mound breakwaters and to reduce repair costs. In order to reduce damages caused by the scour, a protective layer is constructed in front of the breakwater. In this way, the scour can not be completely prevented but can be minimized. The protective layer consists of only the part called berm or berm with apron. The apron should be designed to protect its structure against scour, wave, and current effects. It is important to determine the width of the protective layer, *l*, and the number of layers, *N*, at the design stage.

On the other hand, Sumer and Fredsøe (2000) suggested the *l*, must be at least equal to the width of the scour hole, *W*, for the trunk section. Otherwise, some scour can occur in front of the breakwater. The number of layers in the protective layer is considered necessary since the stones in the layer will fill the scour hole. Figure 3.16 displays the experimental test results of Sumer and Fredsøe. As a result of their experimental studies, they accomplished that the relative scour depth decreased from the order of 0.7 to the order of 0.3 for the trunk section. As the number of layers, *N*, increases, scour decreases.

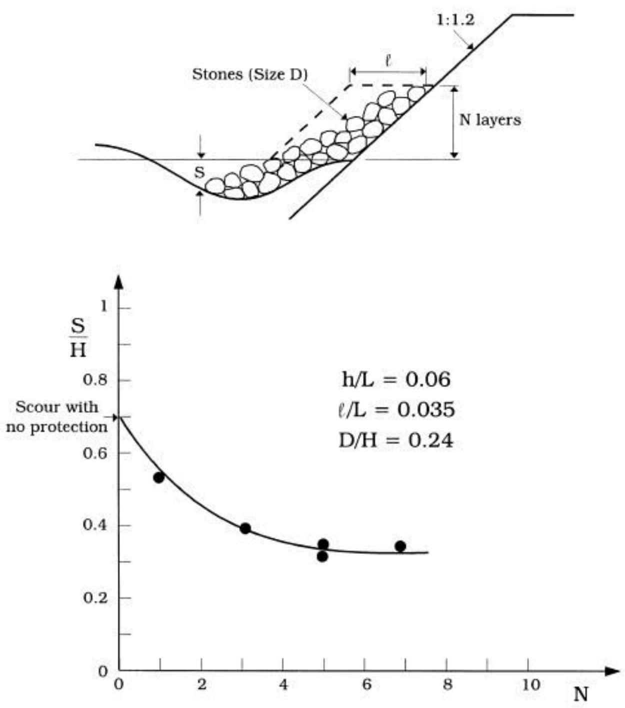

Figure 3.16 The relation between the number of layers and the scour. No-suspension mode. Sumer and Fredsøe (2000)

When it comes to the head section, Sumer and Fredsøe (2002) suggested width for the protective layer is,

$$\frac{l}{B} = A_1 KC \tag{3.7}$$

where the coefficient A_1 = 1.5 for a whole protection (S/B =0) and A_1 = 1.1 for S/B ≤ 0.01. Notice that the dimension of the l is the same as KC number. It means that lee-wake vortices's influence area on the seabed must be covered by the protective layer. Plan view of the protective layer in the head section can be seen in Figure 3.17. The data obtained as a consequence of the experiments. In order for scour to be completely eliminated, scour must be filled with a protective layer as can be seen in Figure 3.17. These results supply an important reference for designing a protective layer using the optimum amount of stone material.

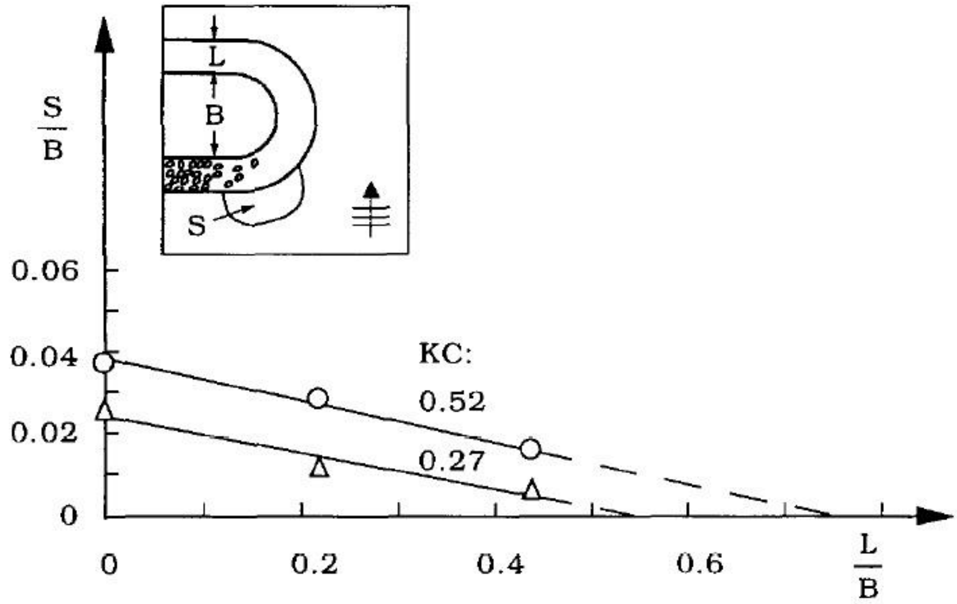

Figure 3.17 Protective layer. B = base width of the rubble-mound breakwater (Sumer and Fredsøe, 2002)

In their study, Sumer and Fredsøe (2000) came to the following conclusions regarding scour in the trunk section:

- As the side slope decreases, the scour depth decreases.

- The scour depth decreases in case of irregular waves.
- The two-dimensional scour in the trunk section occurs in the form of scour and deposition areas parallel to the breakwater.
- The scour in front of the rubble-mound breakwater is smaller than the vertical-wall breakwater.
- Toe protection against scour can be provided by a protective layer, and for whole scour protection, the width of the layer should be equal to the width of the scour hole experienced on the breakwater without the layer.
- As can be understood from Figure 3.15, the scour depth decreases as *h/L* increases.

3.3 Mode of Sediment Transport

The scour and deposition pattern is based on mode of sediment transport according to Sumer and Fredsøe (2002). There are two different types of sediment transport: suspension and no-suspension mode. The mode of sediment transport essentially depends on two different parameters: Shields parameter, θ, and fall velocity to friction velocity ratio, w/U_{fm}. Equation 3.8 must be fulfilled in order for sand particles to remain in the suspension mode on seabed.

$$\theta\left(\frac{{U_{fm}}^2}{g*(s-1)*d_{50}}\right) > \theta_s\left(d_{50} * \frac{U_{fm}}{v}\right) \tag{3.8}$$

where

U_{fm}: the maximum friction velocity

v: kinematic viscosity

θ_s: shields parameter necessary for the starting of suspension from the bed

This condition is needed to initiate the suspension of sand grains on the seabed. But, it is not adequate to sustain the suspension. Another condition, w/U_{fm}<1 must be fulfilled (Batchelor,1965, and Bagnold, 1966). To put it more explicitly, the suspension mode can be sustained if the fall velocity is less than the friction velocity. Consequently, if these two conditions are satisfied, the sand is in the suspension mode, if not, it is in the no-suspension mode. As seen in Figure 3.18, sediment particles in the suspension mode correspond to the upper recirculating cells, while sediment particles in the no-suspension mode correspond to the lower recirculating cells. If the sand is fine-grained, it is carried by the waves to higher elevations. This corresponds to the upper cells in Fig. 3.18. If the sand is coarse, it is in the no-suspension mode. This corresponds to the lower recirculating cells in Fig. 3.18.

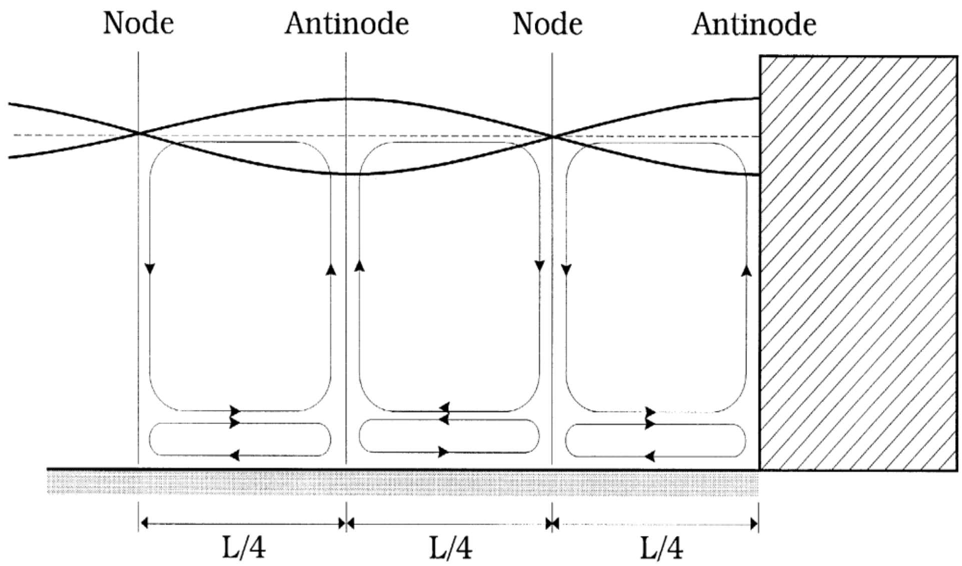

Figure 3.18 Standing wave and recirculating cells (Sumer and Fredsøe, 2000)

On the other side, Xie (1981) introduced a different benchmark for sand transport. He stated that in the case of $(U_m-U_{cr})/w \geq 16.5$, the sand grains are in the suspension mode, otherwise, the sand grains are in the no-suspension mode. Irie and Nadaoka (1984) showed a similar approach to Xie's study.

Sumer and Fredsøe (2000) examined waves acting on the vertical-wall and rubble-mound breakwater. Comparisons were made between these two different types of the breakwaters. As a result, they concluded that the equilibrium scour depth occurring in front of the vertical-wall breakwater was greater. Scour/deposition appears to occur essentially in the same way for both breakwaters, but there are some differences between these two situations.

Firstly, while the scour depth is zero on the vertical-wall breakwater surface, it takes a non-zero value for the rubble-mound breakwater. For a vertical-wall breakwater, the value of the scour depth is zero since there is no steady streaming on the breakwater surface. The fact that a significant scour has occurred on the surface of the rubble-mound breakwater reveals that steady streaming must be taken into consideration in the scour studies. This situation is associated with the inclined surface of the breakwater.

Second, for a vertical-wall breakwater, a significant scour below the 'anti-node' point does not occur. However, for a rubble-mound breakwater, the scour can take a large value at this location. No clear explanation for this behavior has been found. As given in Fig. 3.19, the scour depth in the breakwater goes up to 6 cm. On the other hand, scours can be seen at the 'anti-node' points.

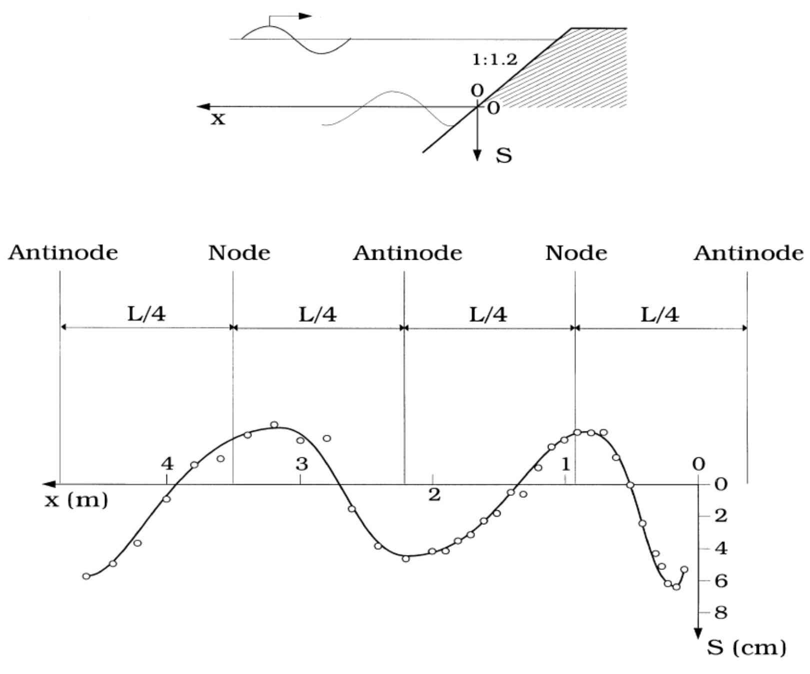

Figure 3.19 Seabed profile. No-suspension mode (Sumer and Fredsøe, 2000)

Third, the maximum scour depth is about 25% smaller in the rubble-mound breakwater case. Since, the flow is weaker due to smaller reflection. Therefore, the equilibrium scour depth is smaller than in the case of a vertical-wall breakwater.

Finally, the depositions occur below the nodal points in the same way for both breakwaters. However, it can be seen in Fig. 3.19 that for a rubble-mound breakwater, the maximum scour depth shifts slightly towards the shore side.

CHAPTER FOUR
EXPERIMENTAL SET-UP AND PROCEDURE

The study was performed in an existing open-wave channel in the Hydraulics Laboratory of Dokuz Eylül University. The channel was constructed with a length of 33 m, a width of 3.6 m, and a depth of 1.2 m. In the offshore part of the channel, a plunger-type wave generator was used to form regular waves with various heights and periods. Regular waves are produced in the channel, owing to the mechanical wave generator that produces waves at a certain frequency. The channel ground form around the wave generator, which produces regular waves at a certain frequency, is shown in Figure 4.1. A depth of 25 cm is left to increase the immersion depth of the wave generator. In this way, the necessary immersion depth is provided for the generation of high-frequency regular waves. The wave generator oscillates up and down, causing the movement of the water body from offshore to onshore. As a result, the water surface changes periodically, creating waves.

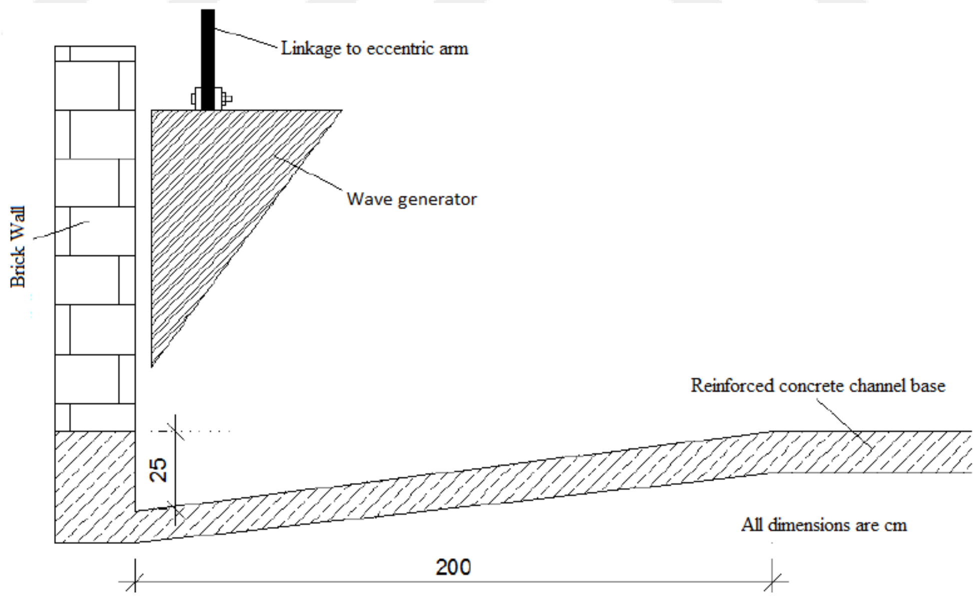

Figure 4.1 Ground form around the wave generator

For the head section experiments, some changes were made in the channel. The width of the sandpit, which has a width of 120 cm and a depth of 17 cm, was increased to 340 cm. In the sandpit expansion process, first of all, the concrete floor was broken by a concrete crusher and the debris was taken out of the channel and taken to the solid waste storage sections in our laboratory. In Figures 4.2 and 4.3, photographs of the crushing process carried out in the sandpit expansion work are given.

Figure 4.2 Breaking the ground to widen the sandpit

Figure 4.3 Expanding the sandpit

After the crushing process is completed, in order to obtain a floor that will withstand the loads that will come, aggregate was laid on the bottom and a steel mesh was placed on it. Then, ready-mixed concrete with the C30 feature was poured into the channel floor in order to obtain a flat ground and the desired depth. Photograph of the steel mesh application is given in Fig. 4.4 and photograph of the ready-mixed concrete pouring process is given in Fig. 4.5.

Figure 4.4 Steel mesh and aggregate laying process

Figure 4.5 Ready-mixed concrete pouring process

After the concrete pouring and screeding processes, it was waited for the concrete to set for three days. Then, sediment was laid in the sandpit, and the head section of the breakwater was formed with the stones used in the trunk section. The head section, which built using limestone to examine the scour, is seen in Figure 4.6. The stones were arranged in such a way that the slope of the breakwater is 1:1.5. In Figure 4.7, the technical drawing of the head section is given.

Before each experiment, some seabed materials with the thickness of d_{50} = 0.23 mm and d_{50} = 0.55 mm were located in the surroundings of the breakwater without any compaction process. After each experiment, the surface of the disturbed bed was arranged to create a flat surface. The seabed materials used in the experimental studies are quartz sand and have a uniform distribution. The median grain diameters of the sands used in the experiments are as follows: 0.55 mm and 0.23 mm for medium and fine grain sizes, respectively.

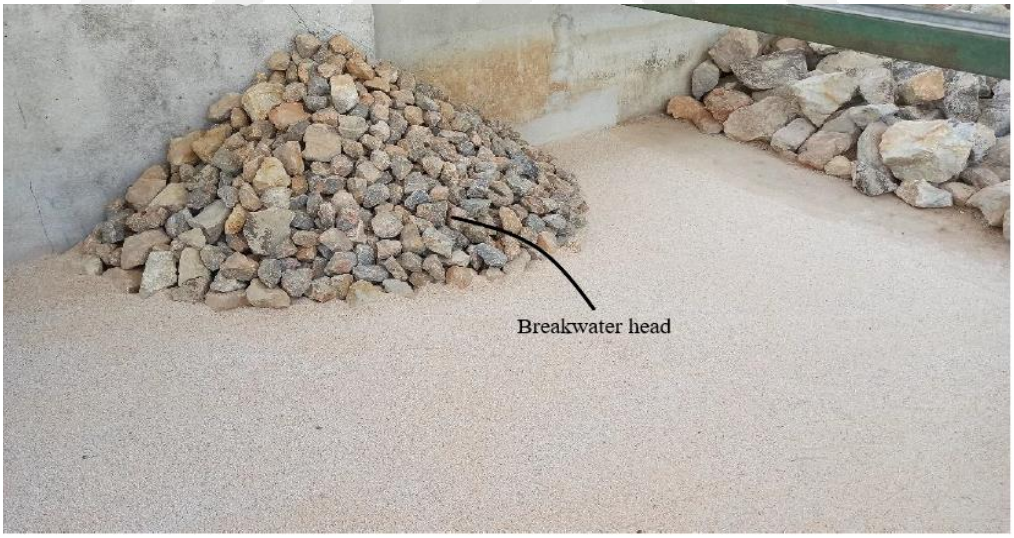

Figure 4.6 Breakwater head in the channel (Personal archive, 2021)

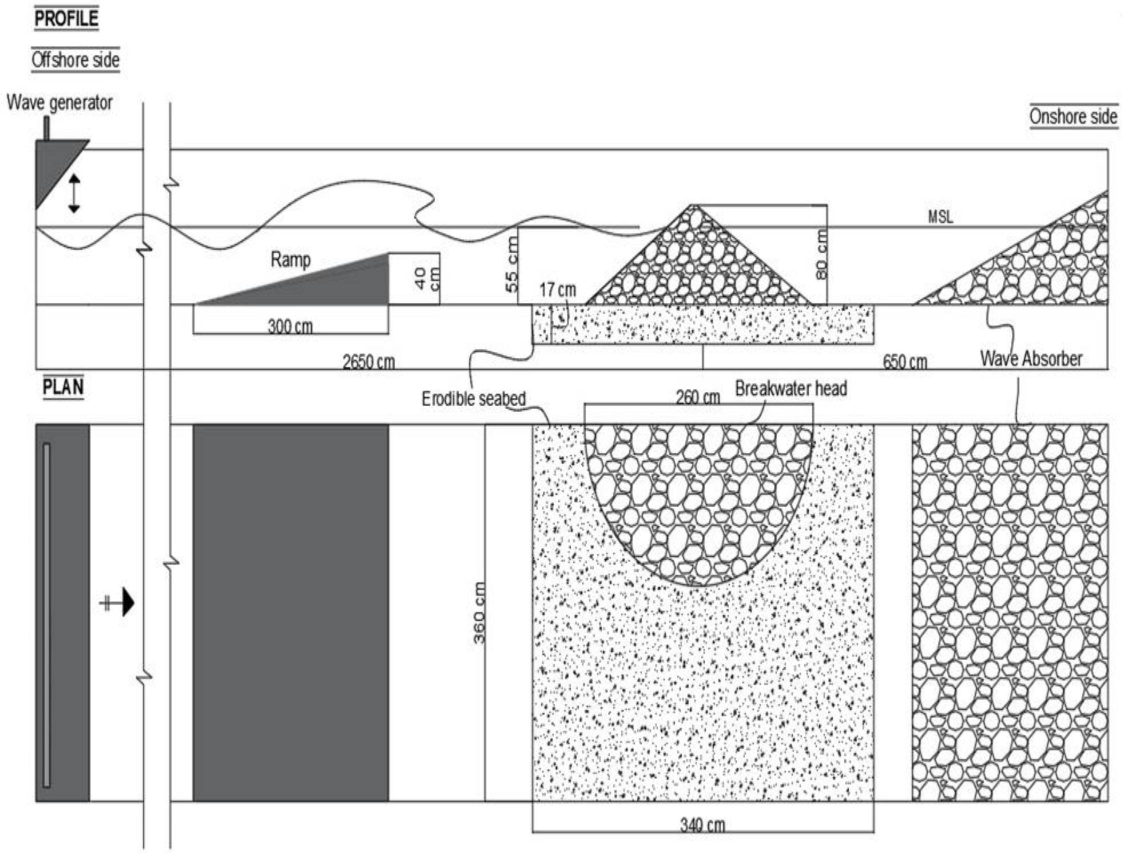

Figure 4.7 Schematic view of the channel

The base of the channel was constructed using reinforced concrete with a thickness of 18 cm. The side walls are made of block bricks placed transversely. Cement-based waterproofing material was applied to the channel surface as insulation material. In addition, 40x60x2 mm box profiles were used every 1.5 m on the outside of the channel to provide resistance to the static and dynamic effects of water. Additionally, observation openings are placed at a distance of 6 m from the onshore side, and dimensions of the openings are 1x1.2 m. Figure 4.8 demonstrates the observation openings. These openings are used to evaluate the water level and to examine the instantaneous state of the scour during the experiments.

Figure 4.8 Observation openings

The trunk section of the breakwater which was used in previous experiments and located on the onshore side, was used to eliminate the reflection of waves produced by the wave generator. It means the trunk section was used for the purpose of wave absorption. Figure 4.9 demonstrates the locations of the breakwater head and trunk section used for the purpose of wave absorption. By the help of its inclined and porous structure, the trunk section absorbs the wave energy and prevents the reflection of the waves.

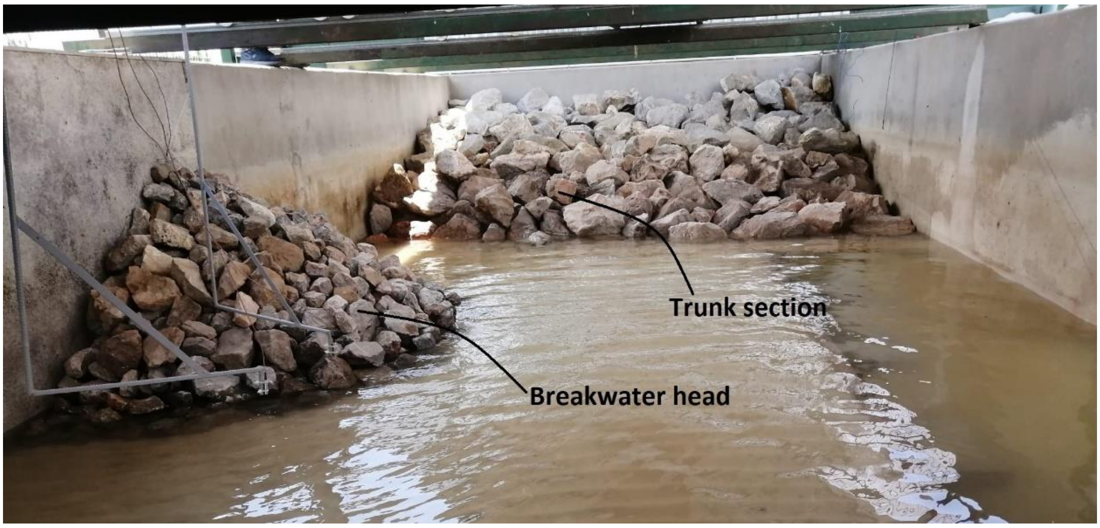

Figure 4.9 Locations of the breakwater head and trunk section in the channel

Experimental scour studies for head section in the case of regular waves acting on the breakwater are basically divided into two as non-breaking and breaking wave experiments. The ramp in Fig. 4.10 was used to create wave-breaking condition before the waves affect the breakwater head. It has a height of 40 cm and a length of 300 cm. The ramp height and width required to create the breaking waves were modeled with the help of the Flow-3D program. In this way, the slope of the ramp that will break all incoming waves has been determined as 2:15. The location of the ramp was demonstrated in Fig. 4.7. Additionally, plunging type breaking is observed at large wave heights, while surging breaking type is observed for smaller wave heights as seen in Fig. 4.11.

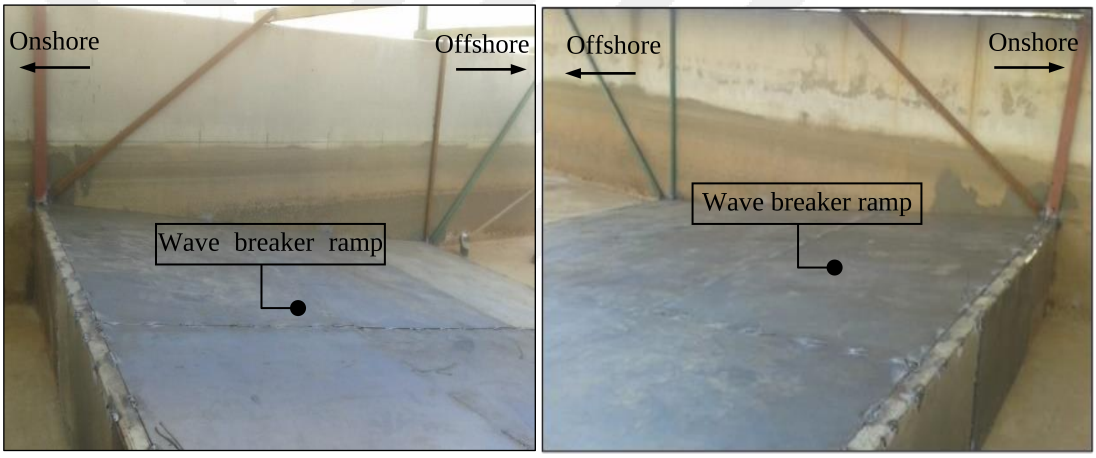

Figure 4.10 Two different views of the wave breaker ramp located in the channel

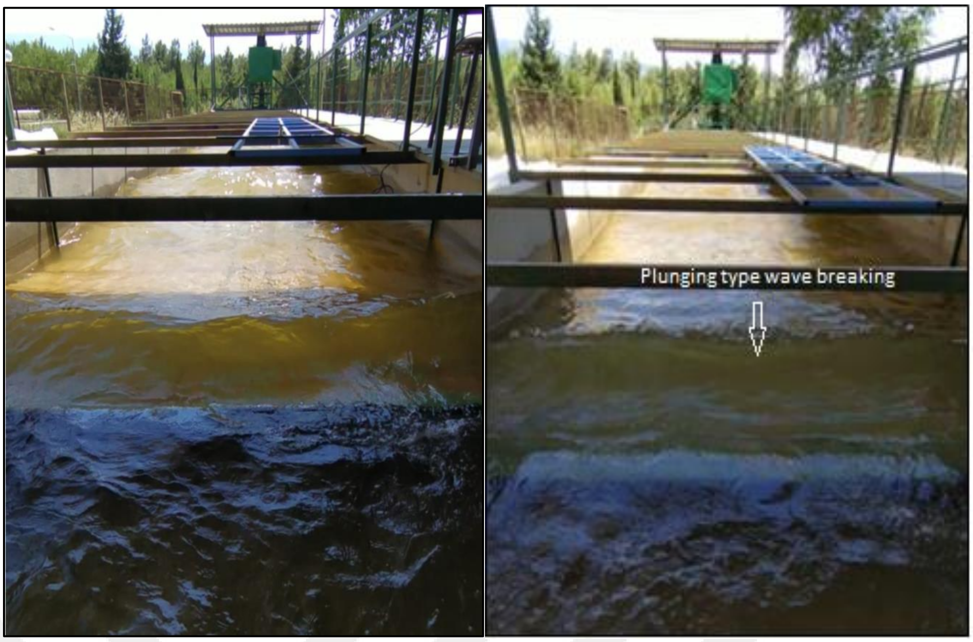

Figure 4.11 Wave breaking in different wave types

The list of experiments performed is given in Table 4.1. Nine of the experiments were investigated experimentally for the breaking case and the remaining nine for the non-breaking case under the same conditions. Furthermore, as given in Table 4.1, four of the nine experiments were performed for sediment particles with d_{50} = 0.55 mm, while the remaining five were carried out for sediment particles with d_{50} = 0.23 mm for both cases.

Table 4.1 Experiments carried out for the head section of the breakwater

Test Number	Wave breaking condition	Wave Period ‘T_W’ (s)	Wave Height ‘H’ (cm)	d_{50} (mm)
B-1	Breaking	1.7	28	0.55
B-2	Breaking	2.7	20	0.55
B-3	Breaking	2.3	22	0.55
B-4	Breaking	3.1	17	0.55
B-5	Breaking	1.7	28	0.23
B-6	Breaking	2.0	25	0.23
B-7	Breaking	2.3	22	0.23
B-8	Breaking	2.7	20	0.23

Table 4.1 Continues

B-9	Breaking	3.1	17	0.23
N-1	Non-breaking	1.7	28	0.55
N-2	Non-breaking	2.7	20	0.55
N-3	Non-breaking	2.3	22	0.55
N-4	Non-breaking	3.1	17	0.55
N-5	Non-breaking	1.7	28	0.23
N-6	Non-breaking	2.0	25	0.23
N-7	Non-breaking	2.3	22	0.23
N-8	Non-breaking	2.7	20	0.23
N-9	Non-breaking	3.1	17	0.23

As measuring instruments, UVP (Ultrasonic Velocity Profiling) and ULS (Ultrasonic Level System) were used (Figure 4.12). The UVP (Ultrasonic Velocity Profiling) device and its integrated sensors are used to evaluate time-dependent scour/deposition depth. The validation of this UVP device was already carried out and published in Guney et al. (2013) In the study, scour and deposition depth measurements were made for different wave periods and seabed materials. During each experiment, scour/deposition measurements were made with the help of UVP at two different points. The positioning of UVP devices is shown in Figure 4.13. One of the UVP devices was placed in the region under the influence of steady streaming where waves approach the breakwater, and the other was placed at the lee-side on which the scour occurs due to plunging breaker.

With the help of the UVP, which works based on the principle that high-frequency sound waves hit a moving particle in the liquid and return repeatedly, the flow velocities along the profile are determined in any cross-section. By using UVP sensors, time-dependent ground movements (scour/deposition) are recorded sensitively. By the help of the UVP device and its associated sensors, scour/deposition depth measurements were successfully carried out in the research projects, 109M637, 111M550, and 215M245, which were completed within the DEU Hydraulics Laboratory. Likewise, my experimental study numbered 218M445, supported by TUBITAK, has been carried out successfully.

It has five different types of sensors that can operate depending on the UVP device. These sensors are categorized according to the frequencies of the sound waves they send. The current types of UVP sensors are those with frequencies of 0.5, 1, 2, 4 and 8 MHz. 20 sensors can be linked to the UVP device simultaneously, provided that the frequencies are the same, and measurements can be taken sequentially. UVP device and 4 Mhz frequency sensors are demonstrated in Figure 4.12-B.

Another measurement tool is the ULS (Ultrasonic Level System) device and USS (Ultrasonic Sound Sensor) sensor. They are used to comprehend the characteristics of the regular waves produced by the wave generator (Figure 4.12-A). The sensors are positioned so that they are perpendicular to the bottom of the canal and do not enter the water.

The sensors are linked to the main device, the ULS, and measure according to the sound wave principle. High-frequency sound waves are sent to the water surface by the sensors. Then, the sound waves reflected back to the sensors can be detected and the vertical distance between the water surface and the tip of the sensor can be calculated. Then, the obtained measurements are transferred to the computer simultaneously.

The height (H_w) and periods (T_w) of the waves in the channel can be figured out exactly from the data in a sensor. The wavelength (L_w) is obtained by simultaneous evaluation of the data of two sensors with a distance of 450 cm between them.

There are two types of USS sensors belonging to the ULS device. One of them is the USS635 and the other is the USS20130 sensors. The numbers next to the USS abbreviation indicate operating ranges in 'cm'. For example, USS635 sensors show that they work when the vertical distance between the sensor tip and the water surface is at least 6 cm and at most 35 cm. Similarly, the USS20130 sensors serve in the range of 20 cm to 130 cm. During the experiments, two USS20130 sensors were used, one located at the position where the breakwater head is placed and the other 450 cm from this position on the offshore side (Fig. 4.13).

Because the water depth was fixed at d = 55 cm in the experiments, five different wave heights were formed in response to five different wave periods. For T_w = 1.7 s (100 Hz), H = 28 cm, for T_w = 2.0 s (87.5 Hz), H = 25 cm, for T_w = 2.3 s (75 Hz), H = 22 cm, for T_w = 2.7 s (62.5 Hz), H = 20 cm, for T_w = 3.1 s (50 Hz), H = 17 cm.

The images of Ultrasonic measurement instruments used can be seen in Figure 4.12. ULS 40D device and USS 20130 transducers are shown in Figure 4.12-A, while the UVP device and transducers are shown in Figure 4.12-B. The positioning of all measurement devices is demonstrated in Fig. 4.13.

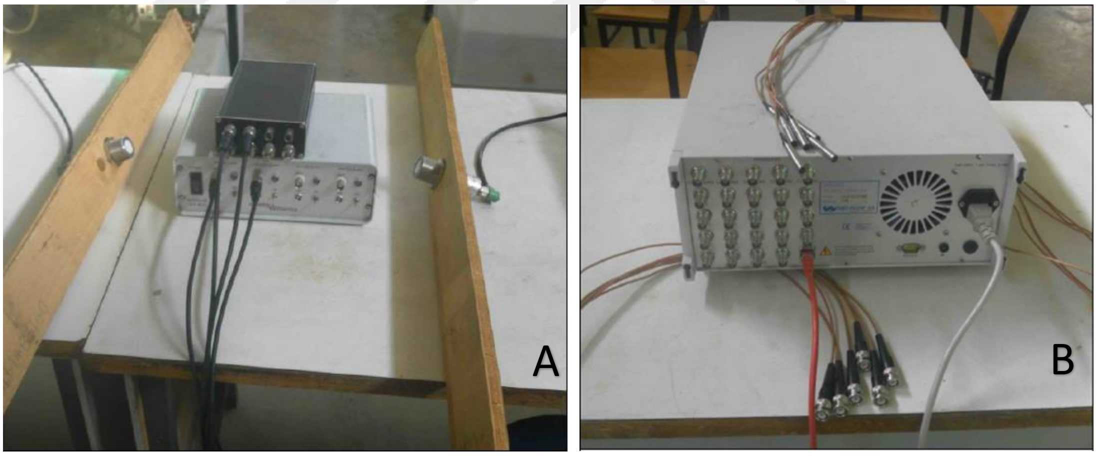

Figure 4.12 Images of ULS 40D device, USS 20130 transducers (A), UVP device, and transducers (B)

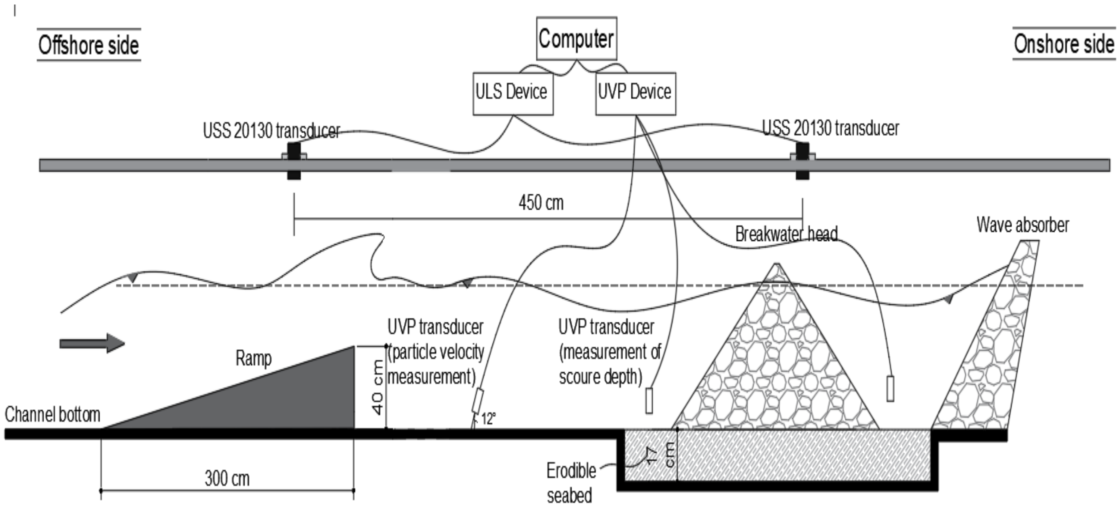

Figure 4.13 Schematic representation of the measuring instruments in the channel

Sieve analysis is a method used for particle size determination of soil particles. In this method, the size distribution of the particles is decided by passing the soil particles through different sizes of sieves. The sieves with different sieve diameters can be seen in Figure 4.14. Sieve analysis can be done for many purposes such as: predicting the quality of soil particles, design of foundations and pavements, determining the fineness modulus of aggregates, etc.

Figure 4.14 Different sizes of sieves (https://dreamcivil.com/sieve-analysis/)

The sieve analysis graph of the bed materials used in the experimental study is given in Fig. 4.15. The bed materials used in the experimental studies are Quartz (SiO_2) sand and have a uniform distribution. Quartz (SiO_2) sand has a specific gravity of γ_s=2.65 t/m^3. As can be seen from the granulometry curves, the median grain diameters are significantly different from each other.

The median grain diameter, d_{50}, is called the diameter that passes 50 percent of the sand grains. To obtain d_{50}, read the value in mm on the x-axis for the value corresponding to 50 % passing on the y-axis of the granulometry curve. If Figure 4.15 is analyzed in this way, d_{50} values can be obtained for fine, medium and coarse sizes.

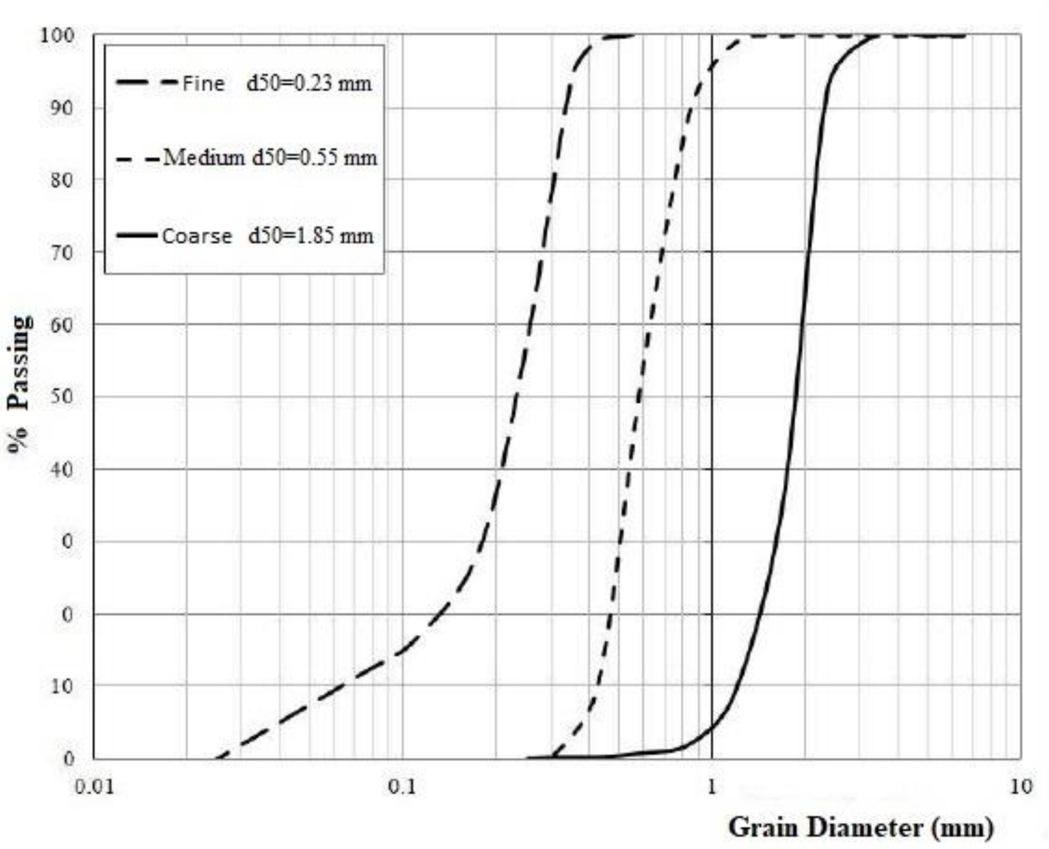

Figure 4.15 The granulometry of the base materials used in the experiments

CHAPTER FIVE
EXPERIMENTAL RESULTS

As a result of the experiments, the ground form was preserved in the head section under the effect of the breaking waves, and a significant scour did not occur. In Table 5.1, the maximum scour depth does not even exceed 17.59 mm. No significant scour occurred in the test results. Although the relative maximum scour depth exceeds 0.03 in Fredsøe and Sumer's experimental study (1997) for the non-breaking wave state, the relative maximum scour depth remains maximum of 0.0068 (S_{max}/B) in our test. This was an expected result because Fredsøe and Sumer (1997) did their study for non-breaking wave state whereas this thesis investigates the breaking wave state. In Table 5.1, UVP_1 represents the relative maximum scour depths measured as a result of the experiment under steady streaming effect, while UVP_2 represents the relative maximum scour depths measured at the lee-side under plunging breaker effect.

Table 5.1 The relative maximum scour depths in the experiments

Test No.	Wave breaking condition	Smax (mm) for UVP_1	Smax (mm) for UVP_2	Smax/B for UVP_1	Smax/H for UVP_2
B-1	Breaking	2.07	6.21	0.0008	0.0222
B-2	Breaking	7.24	11.38	0.0028	0.0569
B-3	Breaking	0.00	11.38	0.0000	0.0517
B-4	Breaking	4.14	1.03	0.0016	0.0061
B-5	Breaking	9.31	14.49	0.0036	0.0518
B-6	Breaking	7.24	7.24	0.0028	0.0290
B-7	Breaking	17.59	7.24	0.0068	0.0329
B-8	Breaking	0.00	14.49	0.0000	0.0725
B-9	Breaking	4.14	6.21	0.0016	0.0365
N-1	Non-breaking	N/A	32.08	N/A	0.1146
N-2	Non-breaking	N/A	5.17	N/A	0.0259
N-3	Non-breaking	N/A	25.87	N/A	0.1176
N-4	Non-breaking	N/A	N/A	N/A	N/A
N-5	Non-breaking	17.59	37.25	0.0068	0.1330
N-6	Non-breaking	12.42	21.73	0.0048	0.0869
N-7	Non-breaking	19.66	21.73	0.0076	0.0988
N-8	Non-breaking	N/A	24.84	N/A	0.1242
N-9	Non-breaking	N/A	34.15	N/A	0.2009

The time-dependent scour/deposition graphs obtained from the experimental test results can be seen in between Figure 5.1 and 5.18. In those figures below, it is shown the test results from which UVP device (UVP_1 or UVP_2). In addition, the numbers greater than zero represent "Scour", while the numbers less than zero represent "Deposition" in those figures.

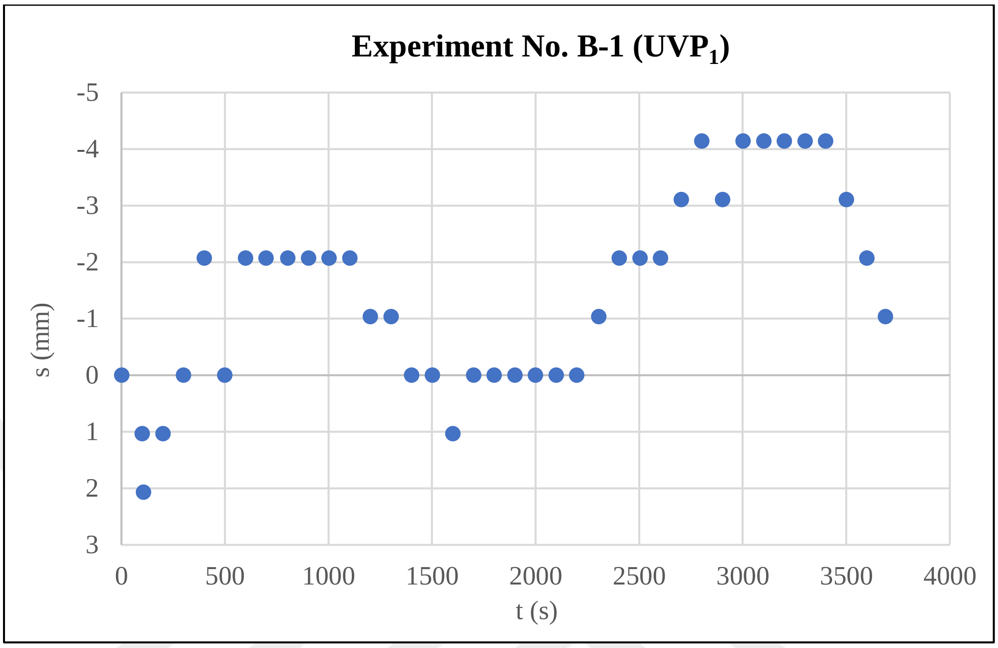

Figure 5.1 Time-dependent scour depths for experiment B-1 (All measurements were taken from UVP_1)

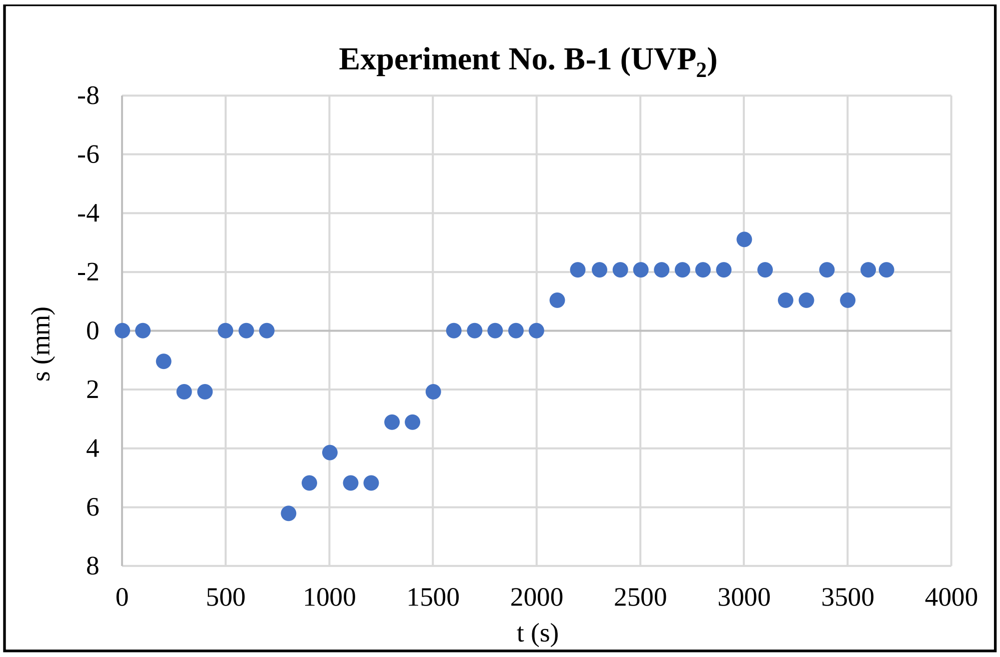

Figure 5.2 Time-dependent scour depths for experiment B-1 (All measurements were taken from UVP_2)

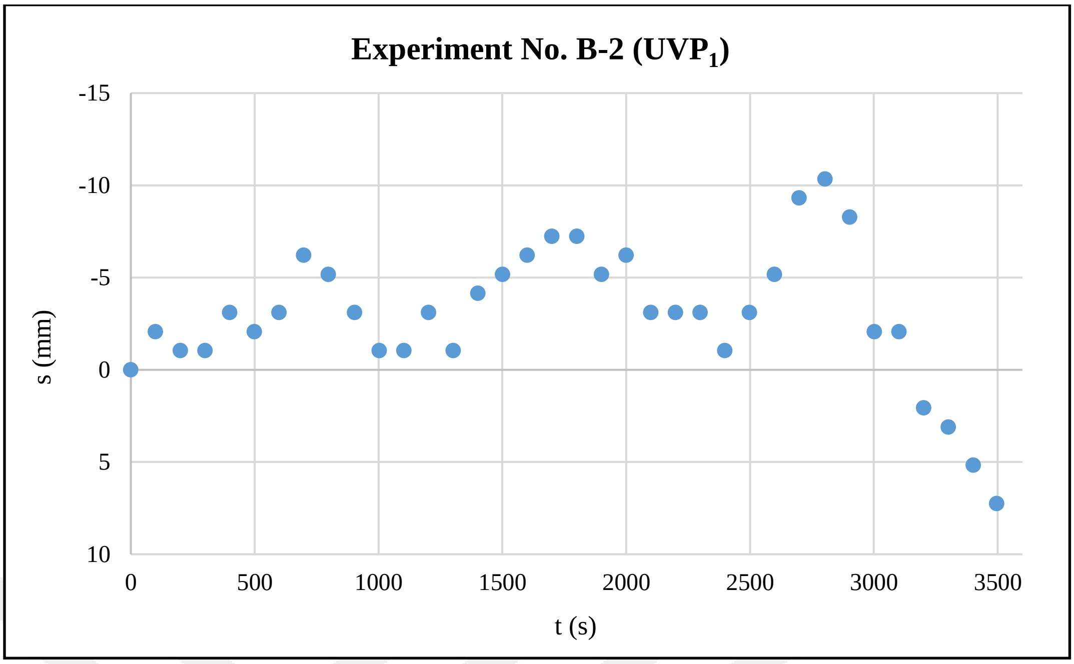

Figure 5.3 Time-dependent scour depths for experiment B-2 (All measurements were taken from UVP_1)

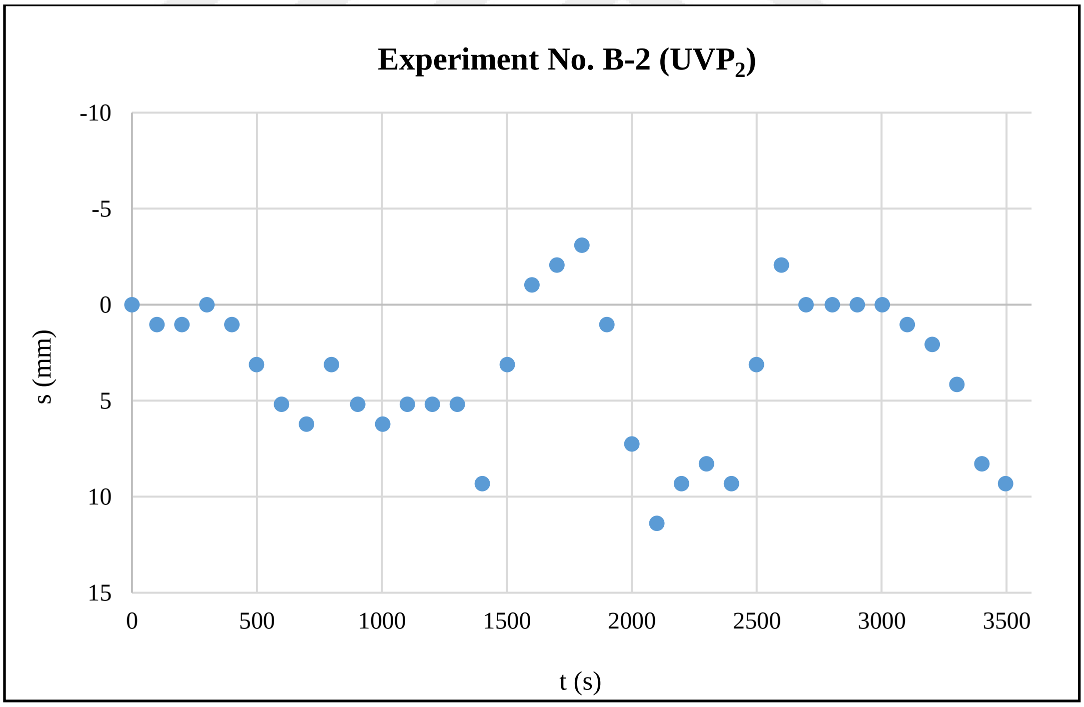

Figure 5.4 Time-dependent scour depths for experiment B-2 (All measurements were taken from UVP_2)

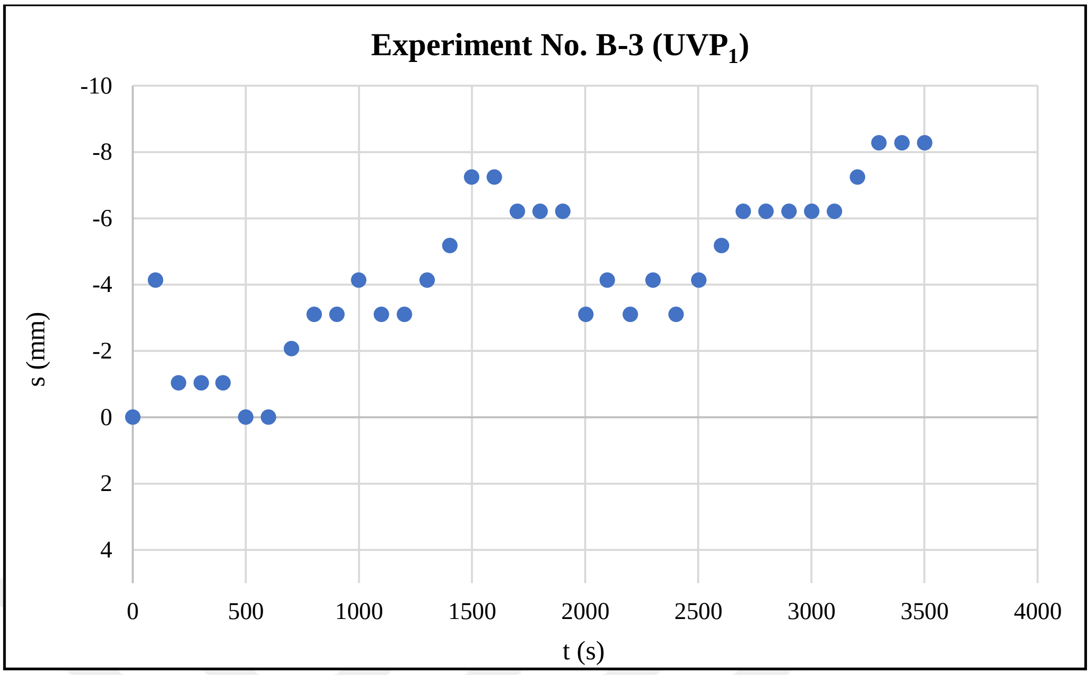

Figure 5.5 Time-dependent scour depths for experiment B-3 (All measurements were taken from UVP_1)

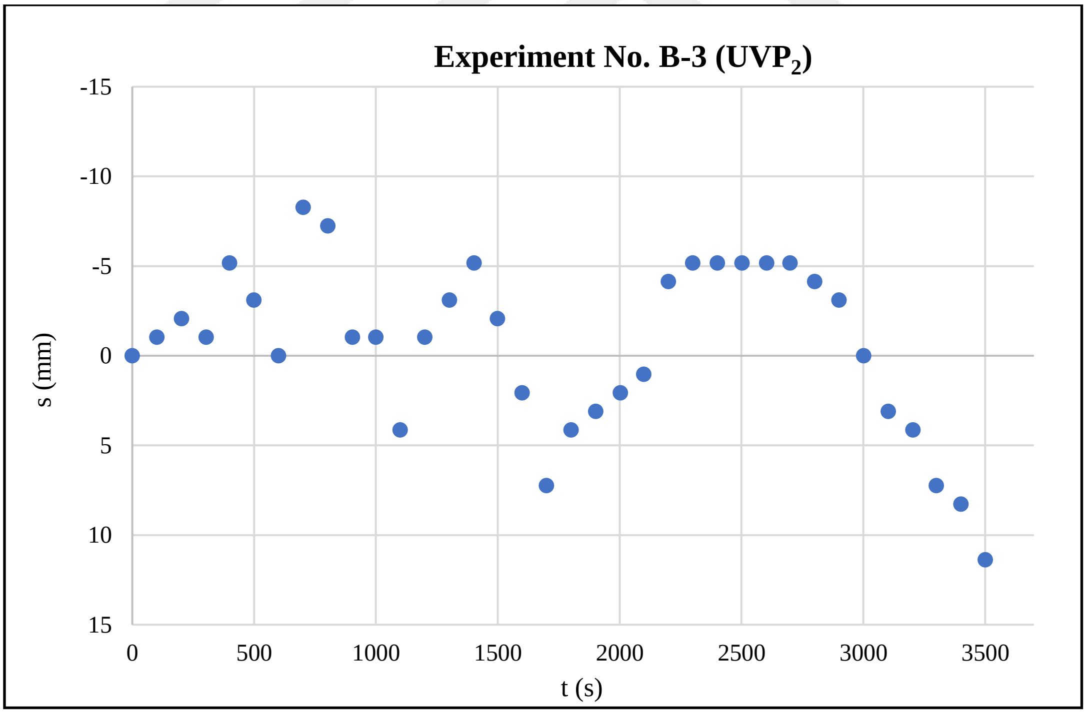

Figure 5.6 Time-dependent scour depths for experiment B-3 (All measurements were taken from UVP_2)

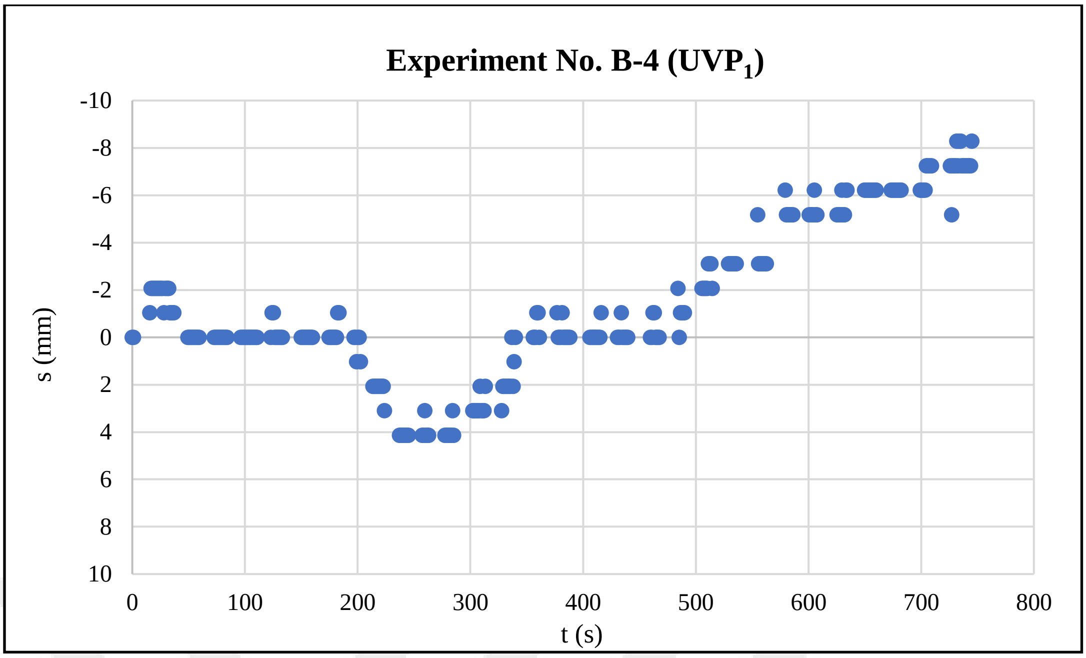

Figure 5.7 Time-dependent scour depths for experiment B-4 (All measurements were taken from UVP_1)

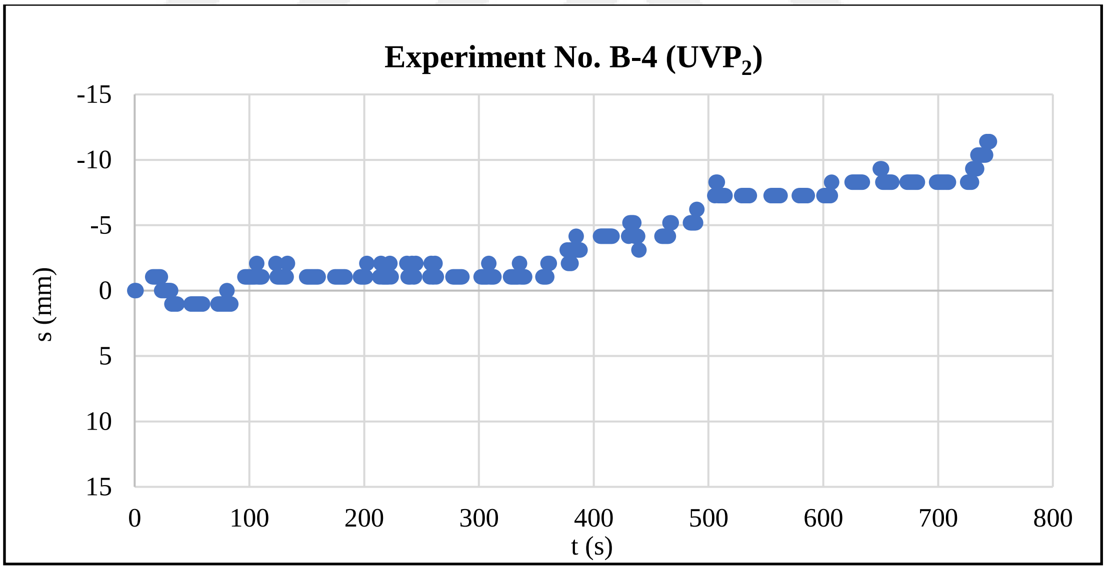

Figure 5.8 Time-dependent scour depths for experiment B-4 (All measurements were taken from UVP_2)

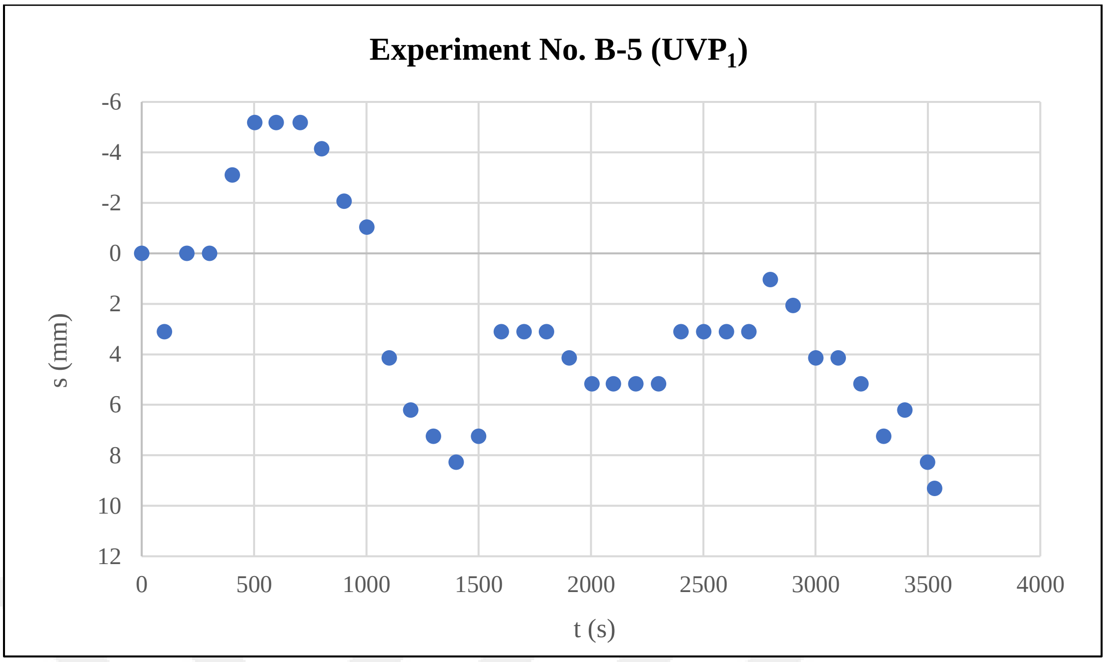

Figure 5.9 Time-dependent scour depths for experiment B-5 (All measurements were taken from UVP_1)

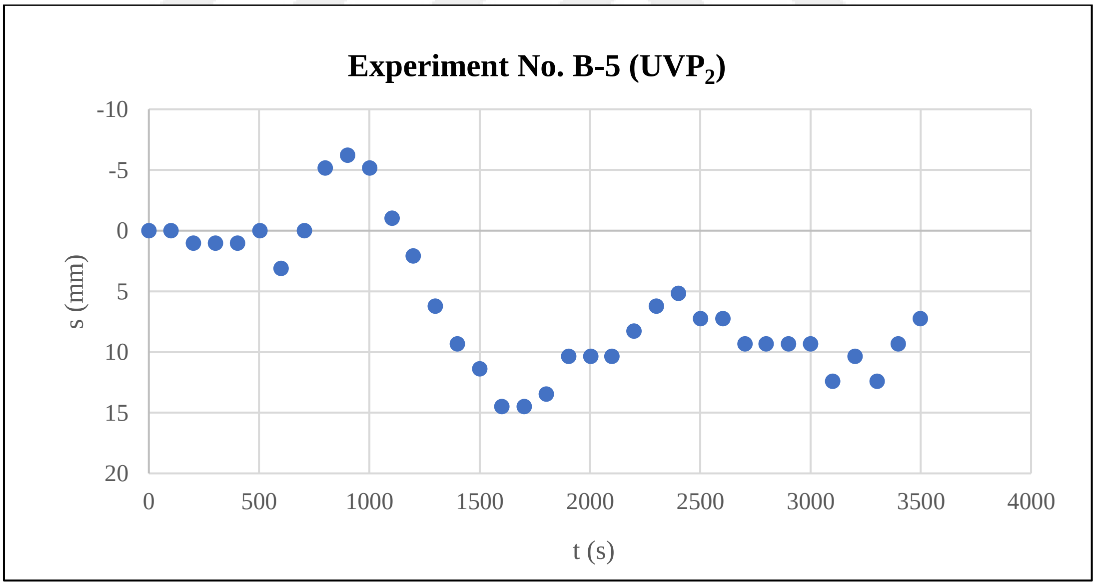

Figure 5.10 Time-dependent scour depths for experiment B-5 (All measurements were taken from UVP_2)

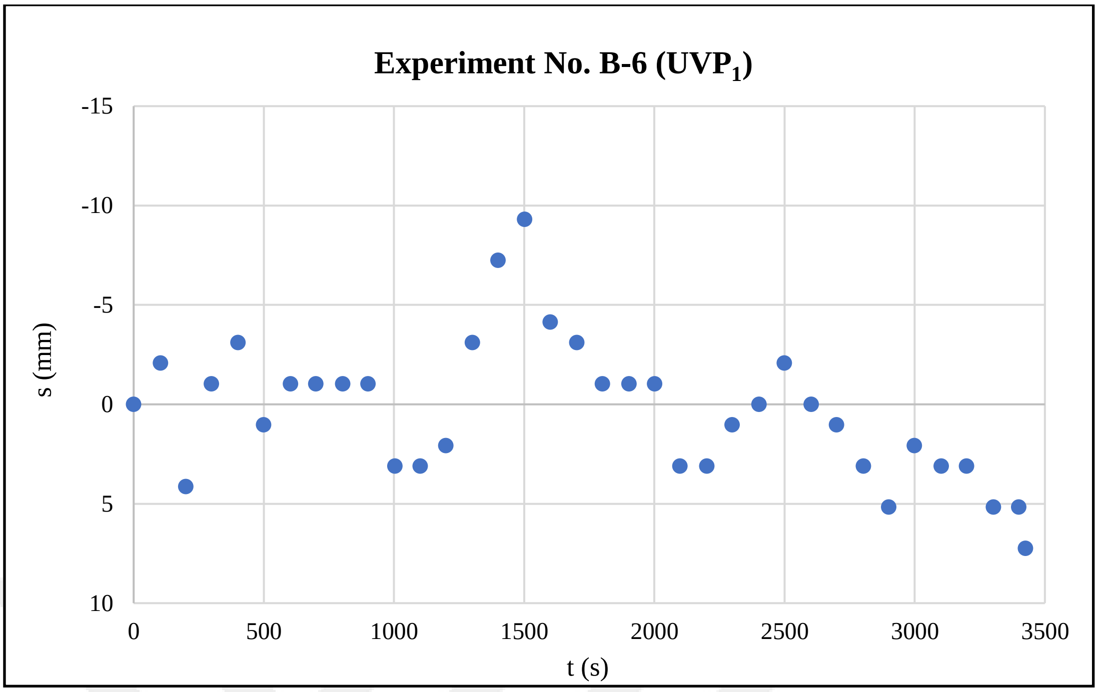

Figure 5.11 Time-dependent scour depths for experiment B-6 (All measurements were taken from UVP$_1$)

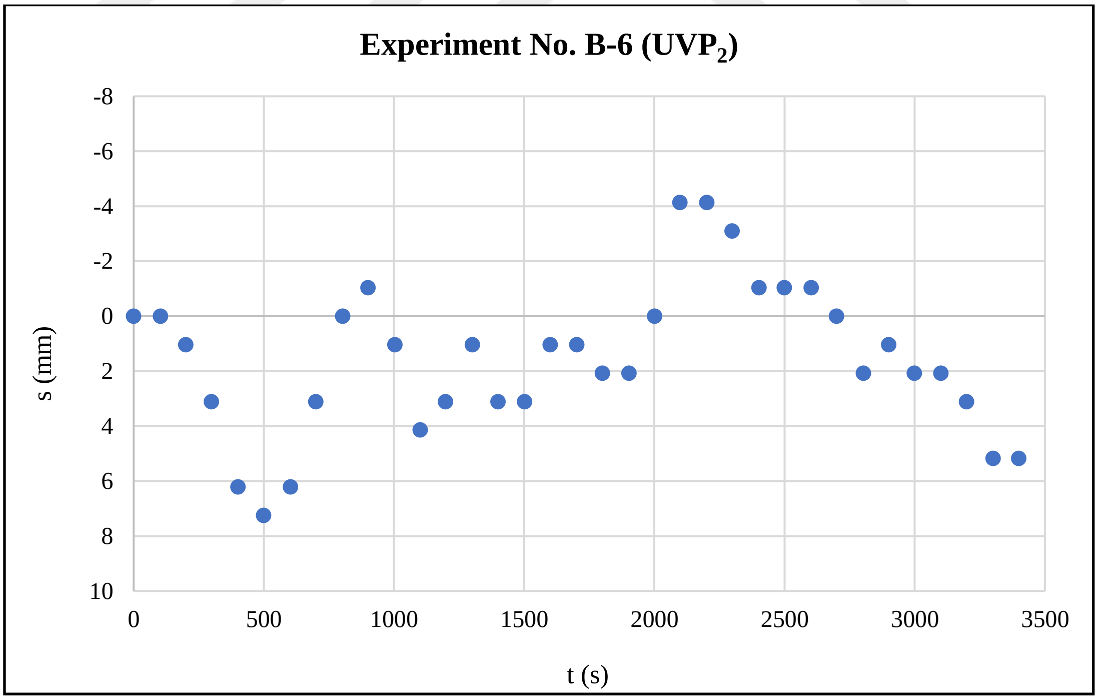

Figure 5.12 Time-dependent scour depths for experiment B-6 (All measurements were taken from UVP$_2$)

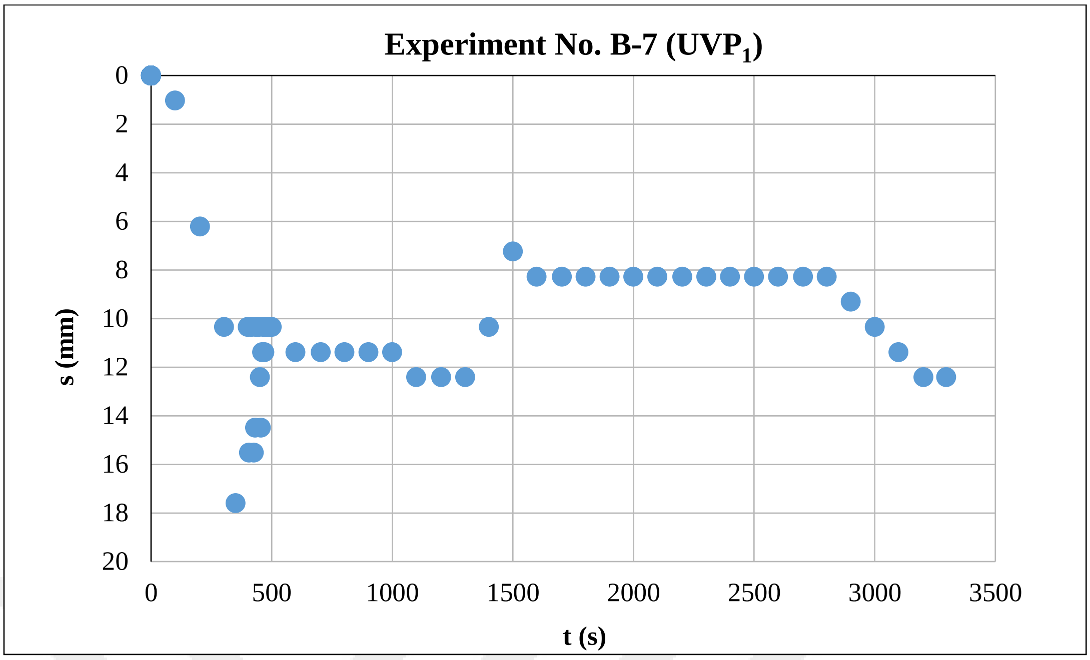

Figure 5.13 Time-dependent scour depths for experiment B-7 (All measurements were taken from UVP$_1$)

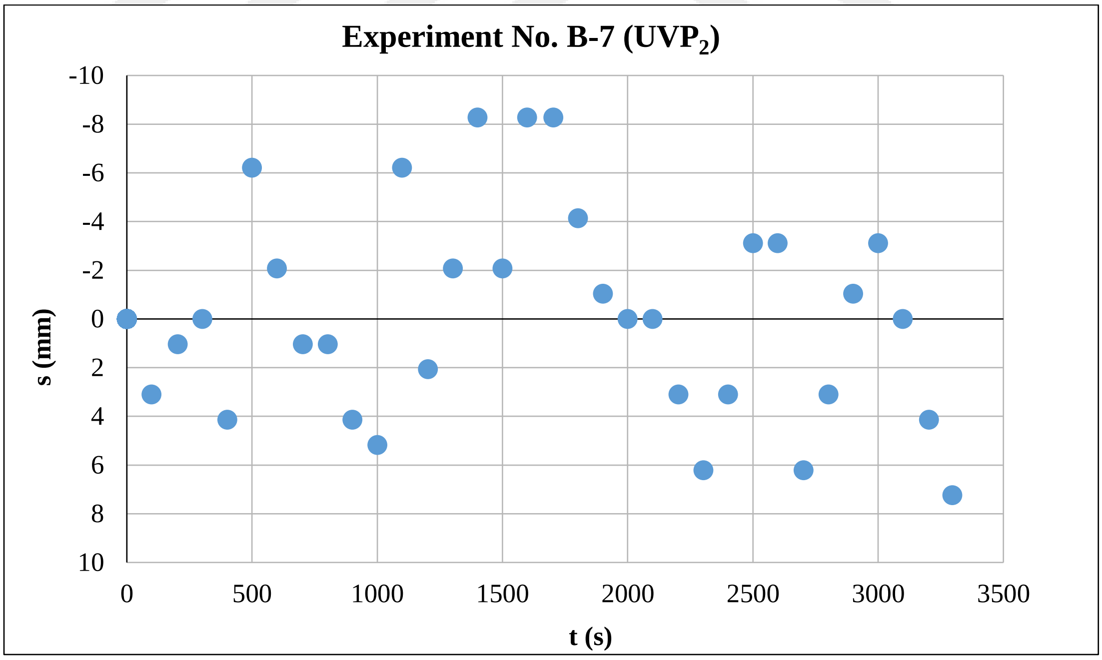

Figure 5.14 Time-dependent scour depths for experiment B-7 (All measurements were taken from UVP$_2$)

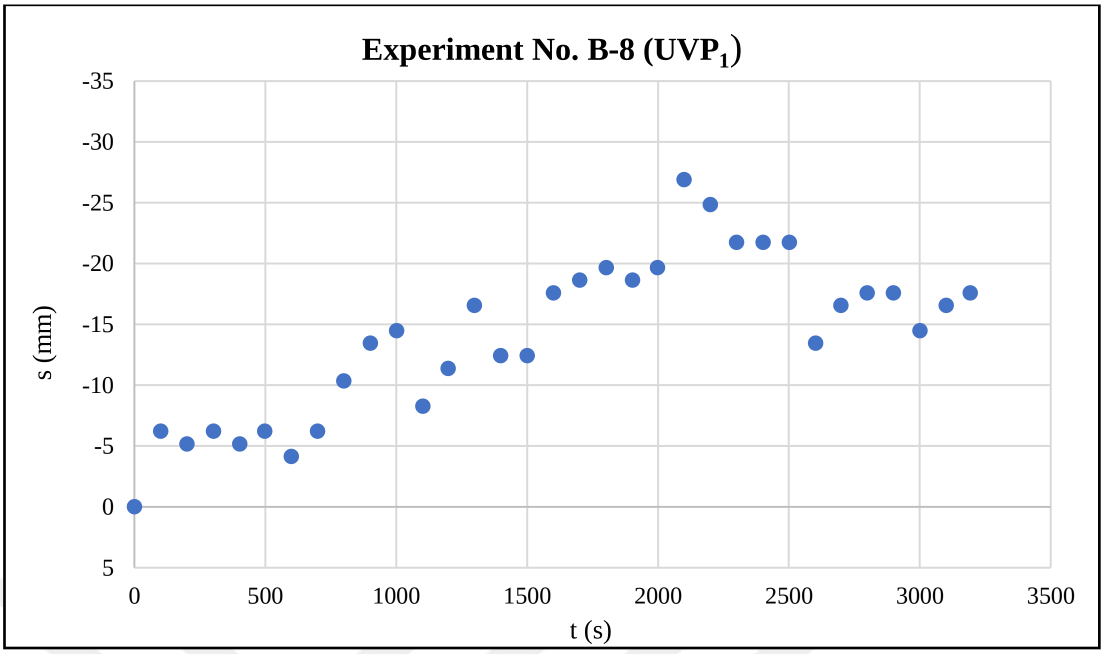

Figure 5.15 Time-dependent scour depths for experiment B-8 (All measurements were taken from UVP$_1$)

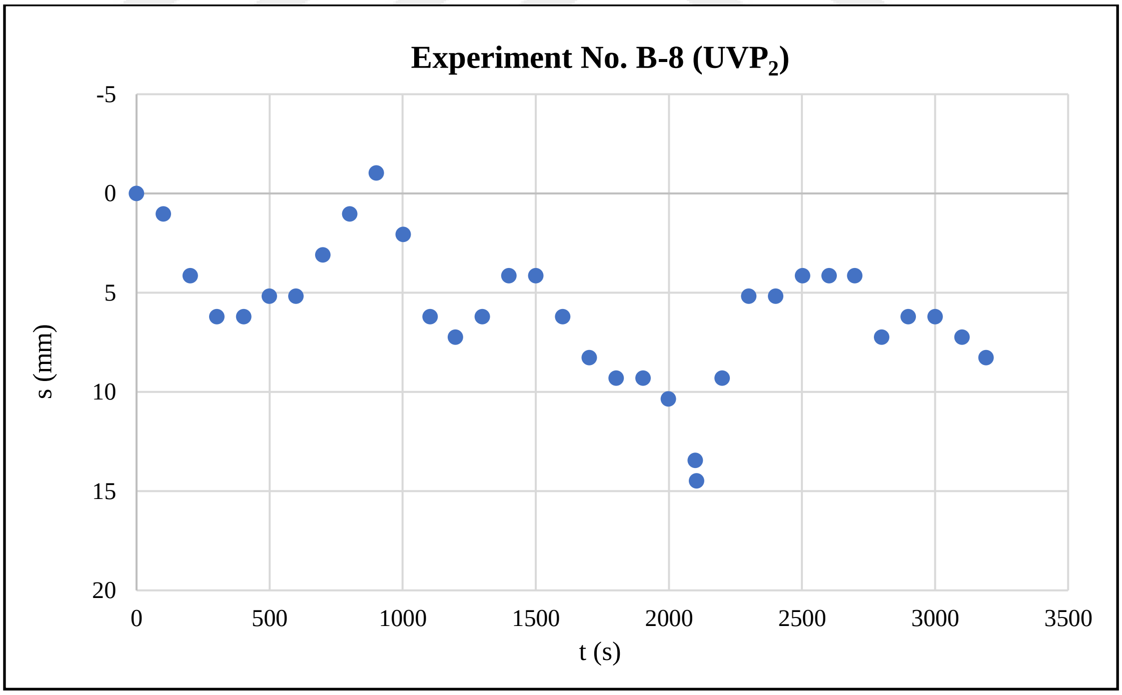

Figure 5.16 Time-dependent scour depths for experiment B-8 (All measurements were taken from UVP$_2$)

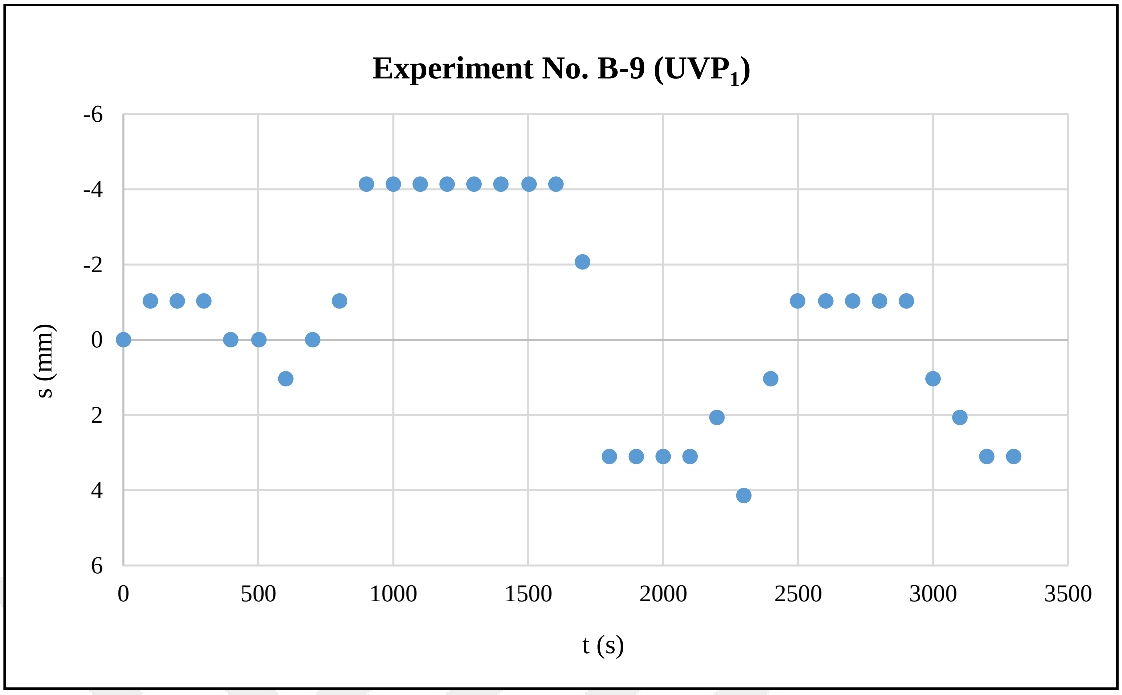

Figure 5.17 Time-dependent scour depths for experiment B-9 (All measurements were taken from UVP_1)

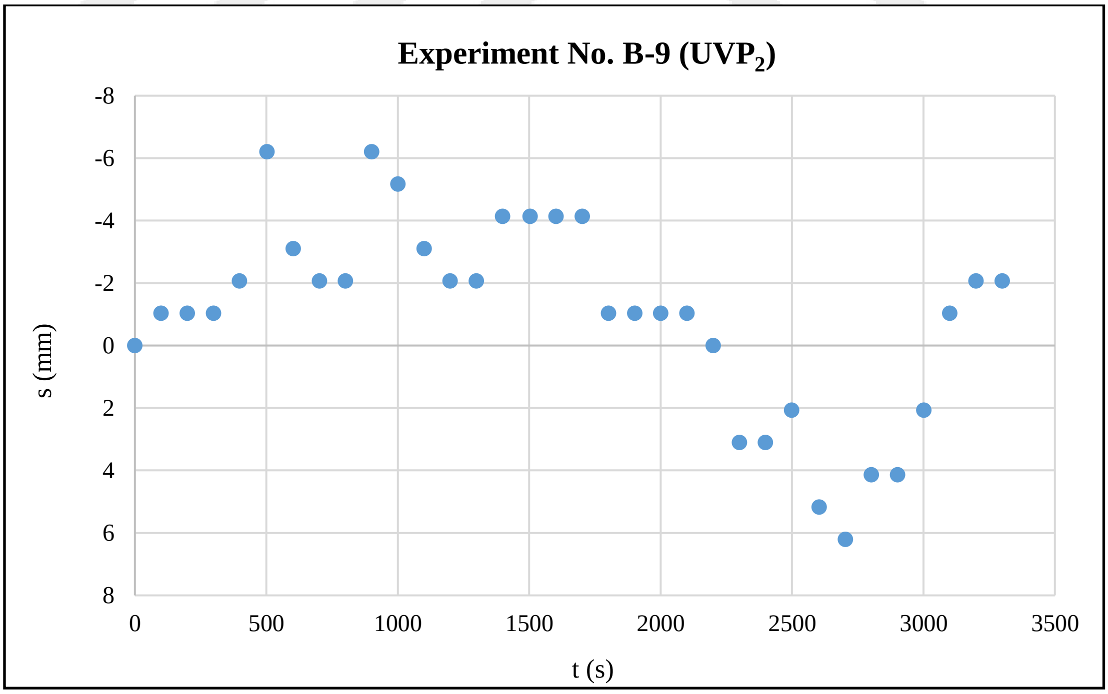

Figure 5.18 Time-dependent scour depths for experiment B-9 (All measurements were taken from UVP_2)

The time-dependent scour depths for breaking and non-breaking wave cases, are given in between Fig. 5.19 and Fig. 5.24. The non-breaking wave data in those figures belong to the experimental studies performed in the same channel previously. This means the time-dependent variation of the scour for both cases was obtained by the same method. There is a significant reduction in scour depths for the breaking wave case compared to the non-breaking wave case as seen from Fig. 5.19 to Fig. 5.24. Since the breaking of waves causes a significant reduction in scour depth, it will be beneficial to pay attention to this situation in the construction process of breakwaters. As can be seen in those figures, experimental measurements took approximately one hour. Since the waves were broken by the help of the ramp, the measurement of the wave reflection could not be performed.

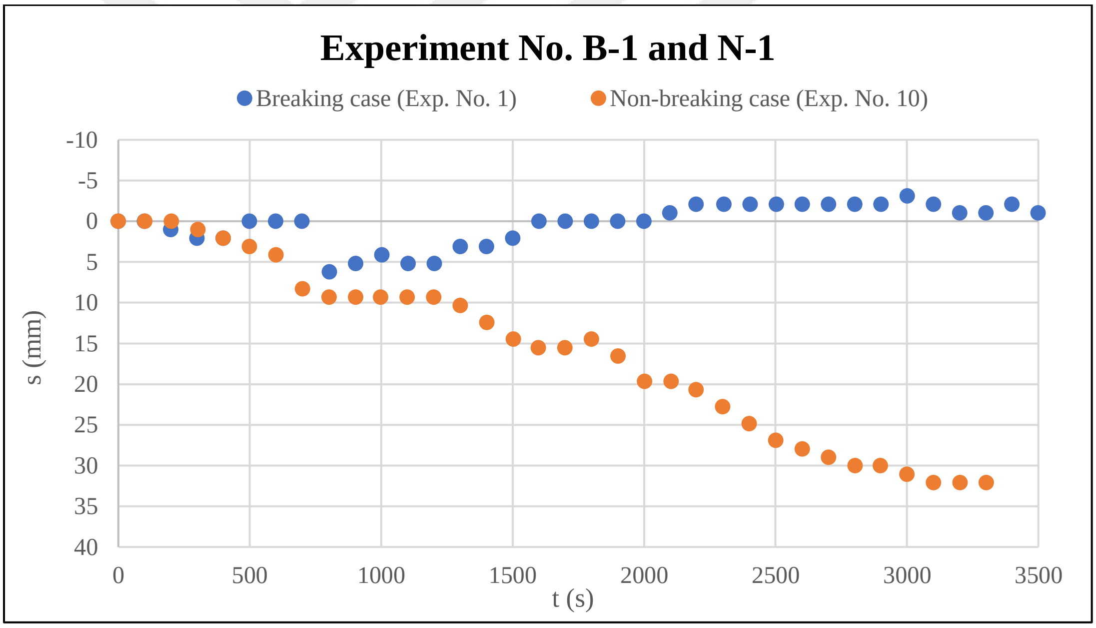

Figure 5.19 Time-dependent scour depths in breaking and non-breaking wave cases. (All measurements were taken from UVP_2 device)

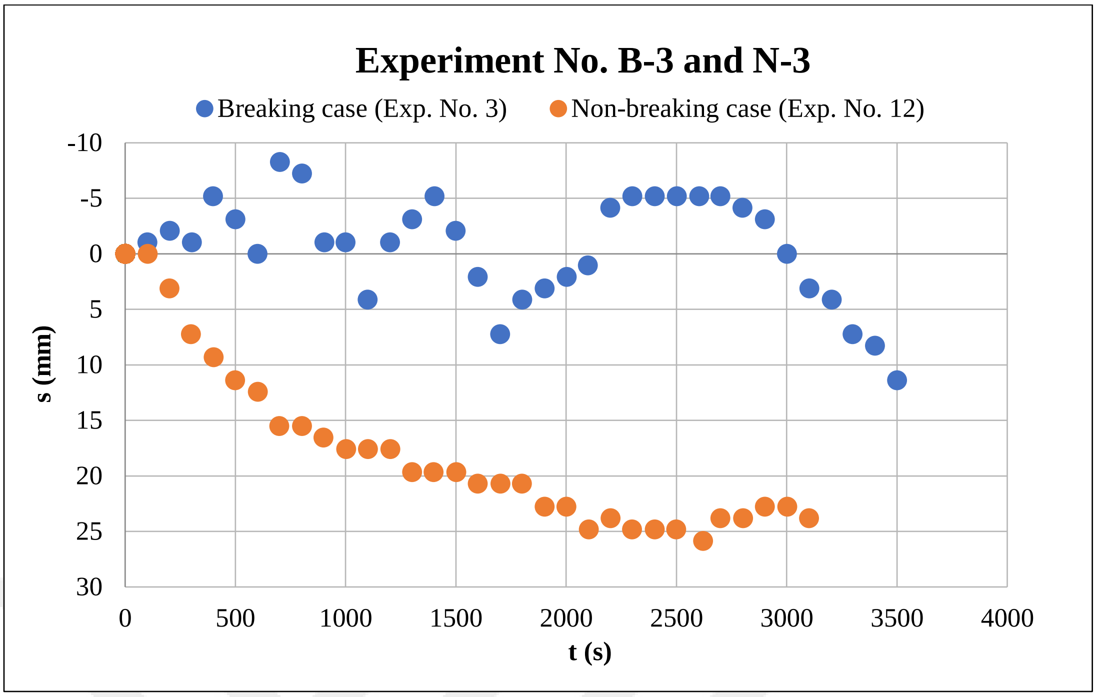

Figure 5.20 Time-dependent scour depths in breaking and non-breaking wave cases. (All measurements were taken from UVP_2 device)

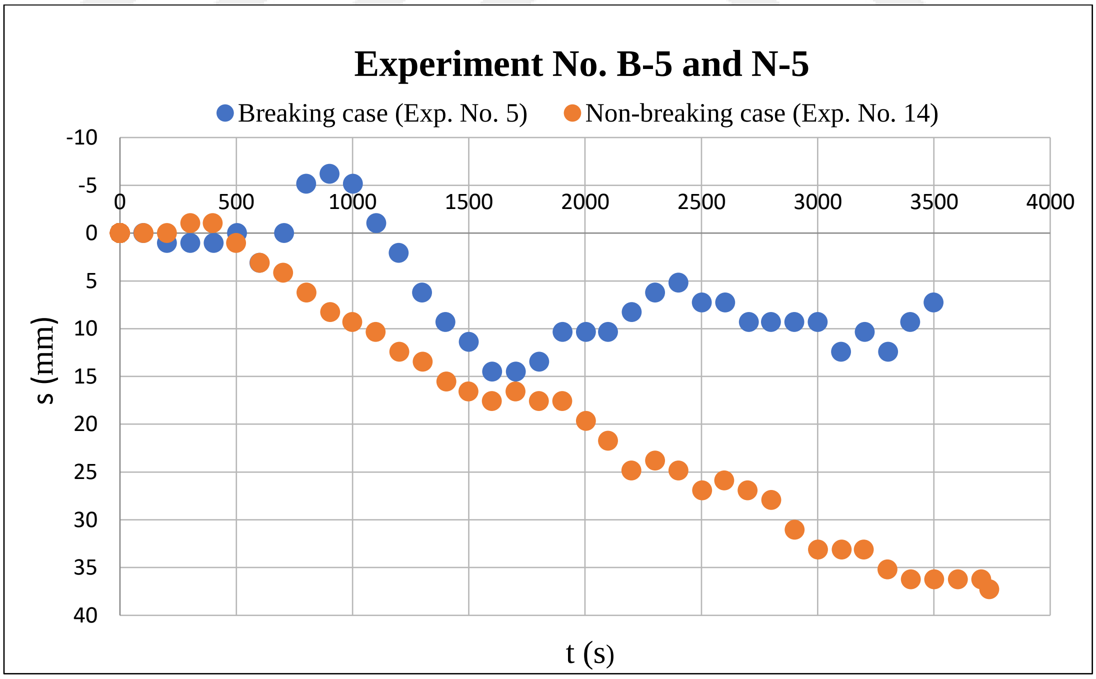

Figure 5.21 Time-dependent scour depths in breaking and non-breaking wave cases. (All measurements were taken from UVP_2 device)

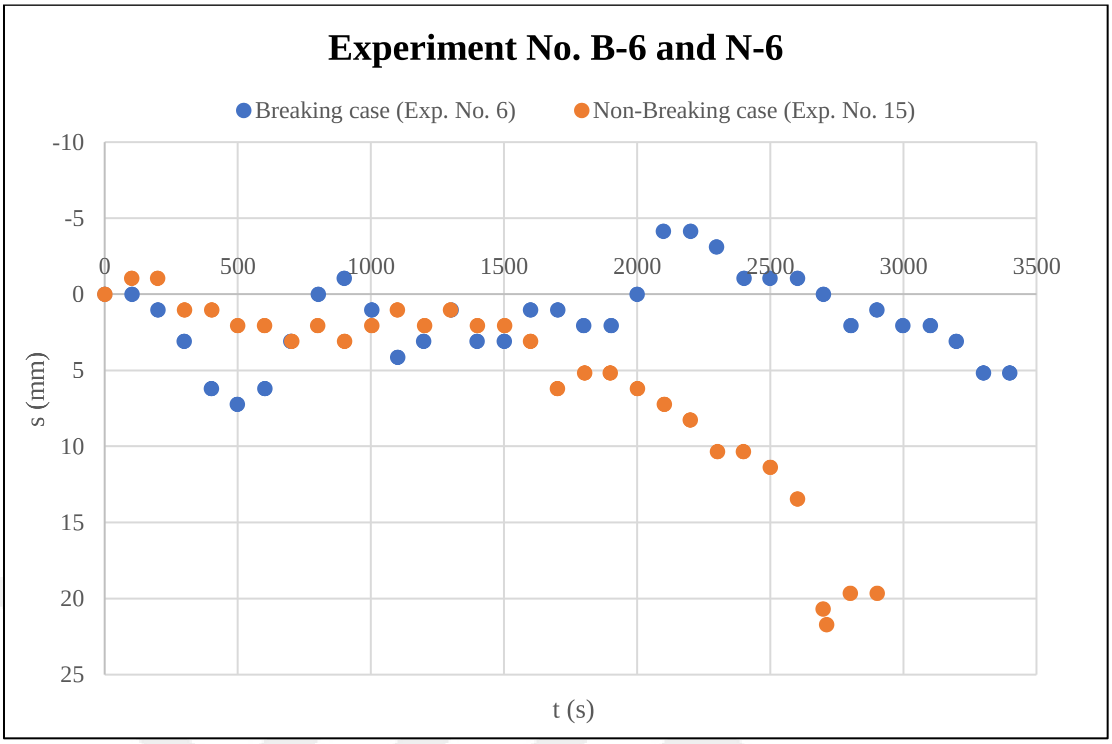

Figure 5.22 Time-dependent scour depths in breaking and non-breaking wave cases. (All measurements were taken from UVP_2 device)

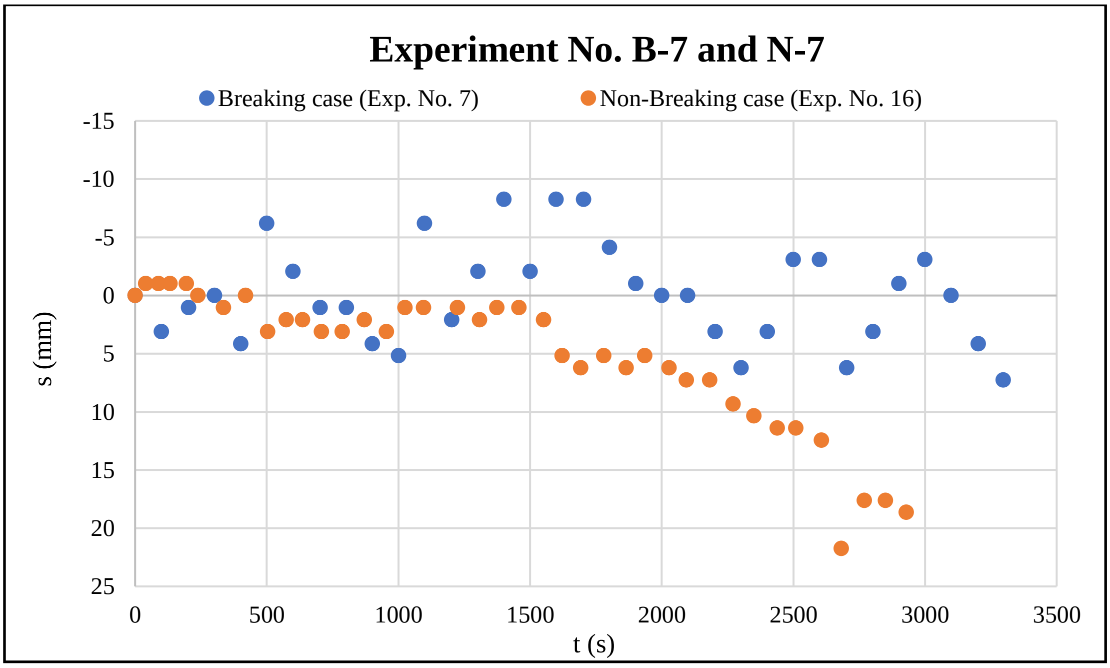

Figure 5.23 Time-dependent scour depths in breaking and non-breaking wave cases. (All measurements were taken from UVP_2 device)

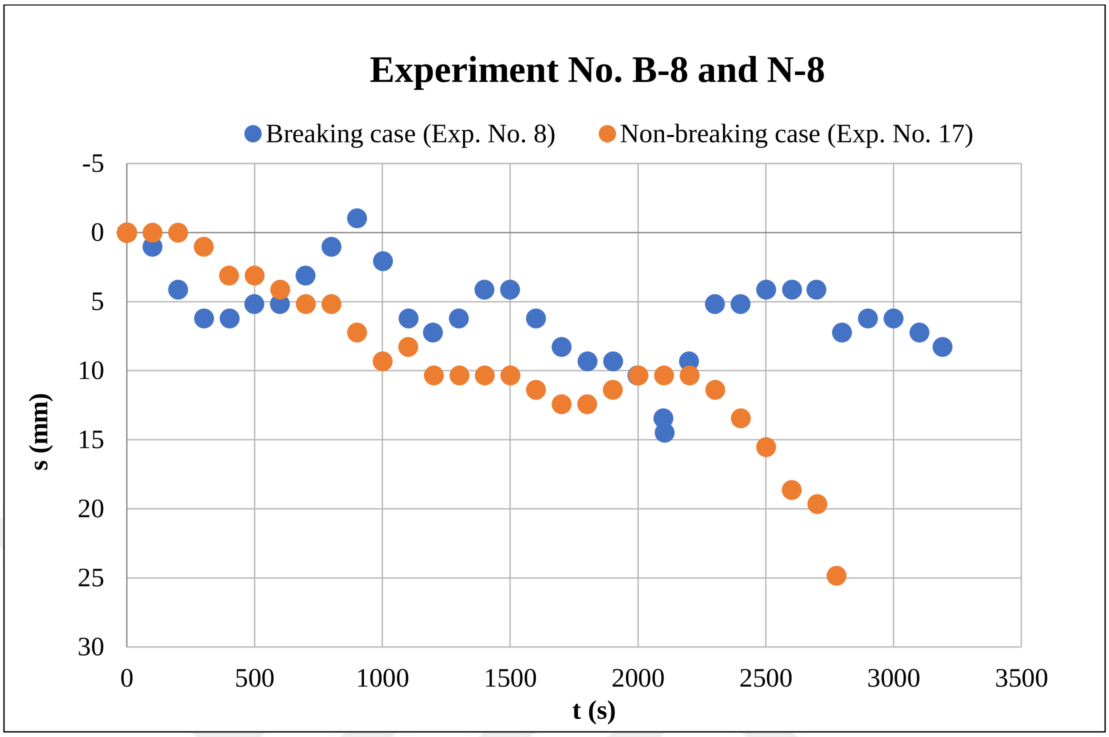

Figure 5.24 Time-dependent scour depths in breaking and non-breaking wave cases. (All measurements were taken from UVP_2 device)

The bed topography around the head section is given in between Figure 5.25 and 5.27. As can be seen, no significant scour is observed and the ground form is preserved around the breakwater for the breaking case. In the non-breaking case, it was observed that the scour caused by plunging breaker reached significant levels. The successive scour/deposition patterns that occur in the head section of the breakwater as a consequence of the breaking and non-breaking wave effect are given in those figures.

Figure 5.25 Bed topography (a) Breaking wave case, (b) Non-breaking wave case, Experiment No. B-1 and N-1

Figure 5.26 Bed topography (a) Breaking wave case, (b) Non-breaking wave case, Experiment No. B-5 and N-5

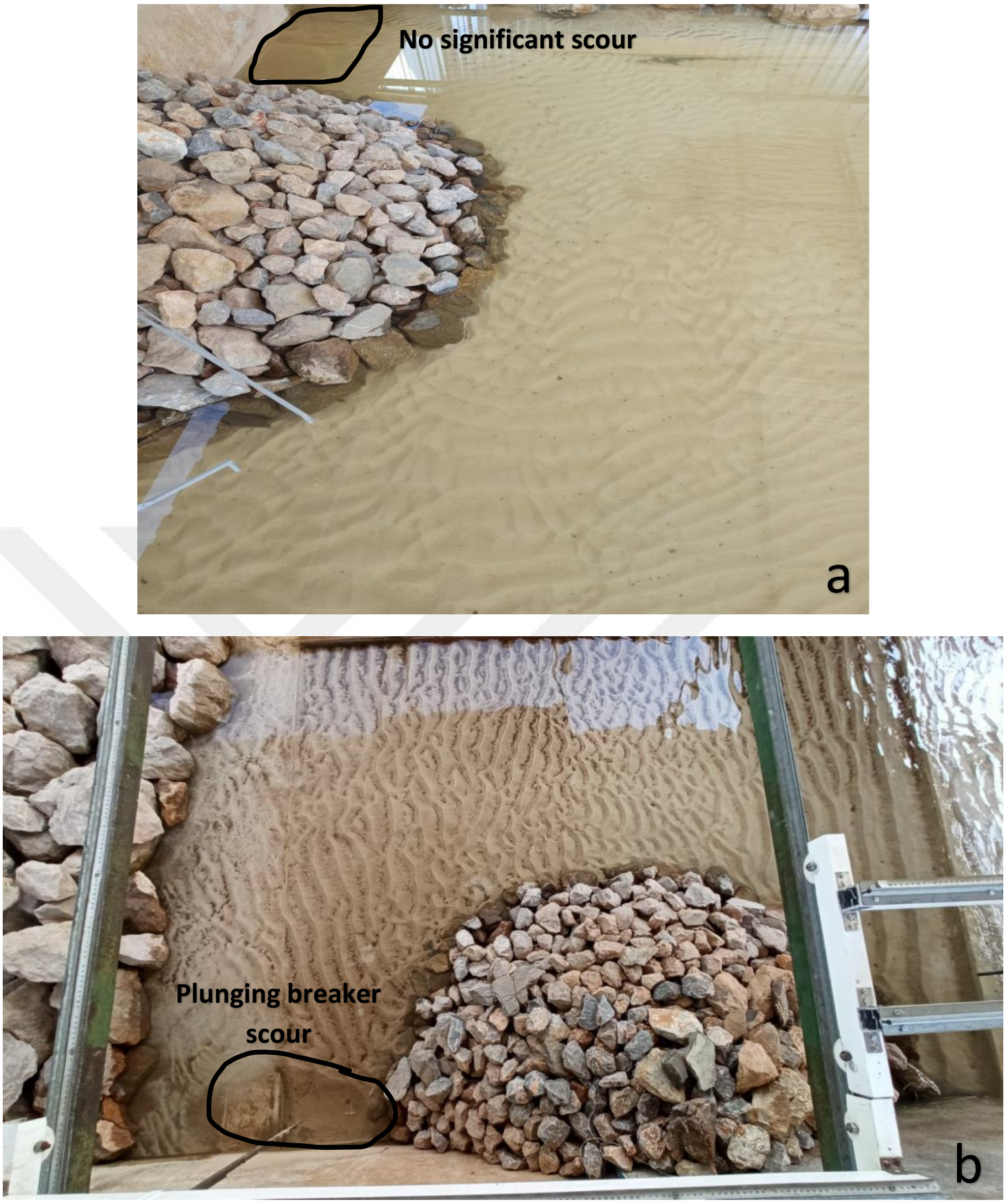

Figure 5.27 Bed topography (a) Breaking wave case, (b) Non-breaking wave case, Experiment No. B-7 and N-7

CHAPTER SIX
DISCUSSION AND CONCLUSION

Within the scope of the thesis, the local scour that occurs as a result of the regular wave effect in the head section of the rubble-mound breakwater were investigated experimentally. Experiments were performed in the open-wave channel within the Hydraulic Laboratory of Dokuz Eylül University. The experiments were performed for a specific surface slope (1:1.5) with two different sandy bed materials (d_{50}=0.23 mm and 0.55 mm), and five different wave periods (1.7, 2.0, 2.3, 2.7 and 3.1 s). The waves produced by the wave generator were broken with the help of a ramp before the model breakwater. Time-dependent scour depths were measured with ultrasonic instruments. In order to determine the propagated wave characteristics and time dependent scour/deposition depths, measurement equipments working with the ultrasonic method were used.

In this experimental study, the deficiency in the literature was eliminated by examining the local scour around the head section for the breaking wave case. In this thesis, local sediment movements were investigated as a result of the breaking and non-breaking wave effects around the head section of a rubble-mound breakwater, experimentally. As a consequence, it was observed that the scour caused by plunging breaker reduced significantly in the case of the breaking wave case. The scour effect of grain diameter, wave period, and surface inclination could not be investigated properly since no significant scour did not occur in case of the breaking waves.

Relative scour depths were obtained by nondimensionalizing the scour depths obtained as a result of the experiments according to the wave height and the base width of the breakwater. From this point of view, the highest relative scour depths obtained from the experiments were compared with the results suggested by Fredsøe and Sumer (1997), and as a result, it was observed that the breaking of the waves significantly reduces the relative scour depths.

The main findings within the scope of the thesis are listed below. As a result of the experimental findings;

- In case of the breaking waves, scour caused by plunging breaker is reduced by 81.8%, while the scour caused by steady streaming is reduced by 47.1%. The decrease in the scour depth at the lee-side of the breakwater (plunging breaker region) is much greater.
- The experimental results in the thesis were compared with the Fredsøe and Sumer's experimental study (1997). While they obtained a relative scour depth of 0.03 under the non-breaking wave conditions, the scour in the thesis remains maximum of 0.0068 (S_{max}/B) in our test.
- The scour caused by plunging breaker reaches serious levels in case of the non-breaking waves. This situation can cause failure of the breakwater.

In addition to this study, which examines the scour formed as a result of the breaking case of the regular waves on the rubble-mound breakwater, examining the breaking case of the irregular waves on the breakwater is recommended as a future work plan in terms of the integrity of the research.

REFERENCES

Arneborg, L., Hansen, E. A., & Juhl, J. (1995). *Numerical modelling of local scour at vertical structures*. Final Proceedings of the project Monolithic (Vertical)\Coastal Structures, Commission of the European Communities, Directorate General for Science, Research and Development, MAST contract No. MAS2-CT92-0042, Paper, 3.

Bagnold, R.A., (1966). *An approach to the sediment transport problem from general physics*. Prof. Paper No.422-I. US Geological Survey. US Government Printing Office, Washington, DC.

Batchelor, G.K., (1965). *The motion of small particles in turbulent flow*. Proc. 2nd Aust. Conf. Hydraul. Fluid Mech. University of Auckland, Auckland, Australia, 019–041.

Burcharth, H. F., & Liu, Z. (1995). *Rubble mound breakwater failure modes.* In Proceedings of the Final (MAS2-CT92-0042) Workshop: Rubble mound failure modes, Sorrento, Italy, November 1995.

Carter, T. G., Liu, P. L., & Mei, C. C. (1973). Mass transport by waves and offshore sand bedforms. *Journal of the Waterways, Harbors and Coastal Engineering Division*, *99*(2), 165-184.

Dally, W. R., Dean, R. G., & Dalrymple, R. A. (1984). *Modeling Wave Transformation in the Surf Zone*. Miscellaneous papers. CERC-84-8, US Army Engineer Waterways Experiment Station, Coastal Engineering Research Center, Vicksburg, 39180-0631.

Dream Civil, (2022, March 20). *Sieve Analysis, 4 Types of Sieves, Lab Procedure, Advantages and Disadvantages, of Sieve Analysis*, https://dreamcivil.com/sieve-analysis/

Fredsøe, J., & Sumer, B. M. (1997). Scour at the round head of a rubble-mound breakwater. *Coastal engineering*, *29*(3-4), 231-262.

Gislason, K., Fredsøe, J., & Sumer, B. M. (2009). Flow under standing waves: Part 2. Scour and deposition in front of breakwaters. *Coastal engineering*, *56*(3), 363-370.

Guney, M.S., Bombar, G., Aksoy, A. Ö., & Dogan, M., (2013). Use of UVP to investigate the evolution of bed configuration. *KSCE Journal of Civil Engineering (SCI-Expanded), 17*(5), 1188-1197.

Hughes, S. A., & Fowler, J. E., (1991). *Wave-induced scour prediction at vertical walls*. ASCE Proc. Conf. Coastal Sediments, *91*, 1886–1899.

Irie, I., & Nadaoka, K. (1984). Laboratory Reproduction of Seabed Scour in front of Breakwater. *Coastal Engineering, 116,* 1715-1731.

Lillycrop, & Hughes (1993). *Scour hole problems experienced by the Corps of Engineers; Data presentation and summary.* Miscellaneous papers. CERC-93-2, US Army Engineer Waterways Experiment Station, Coastal Engineering Research Center, Vicksburg, 39180-6199.

Myrhaug, D., Rue, H., & Tørum, A. (2004): Tentative engineering approach to scour around breakwaters in random waves. *Coastal Engineering, 51*, 1051−1065.

Soulsby, R. L., & Whitehouse, R. J. S. (1997). Threshold of sediment motion in coastal environments. *Pacific Coasts and Ports'97*, *1*, 149-154.

Sumer, B.M., & J. Fredsøe, (2000). Experimental study of 2D scour and its protection at a rubble-mound breakwater. *Coastal Engineering*, *40*, 59-87.

Sumer, B.M., & Fredsoe, J., (2002). *The Mechanics of Scour in the Marine Environment, vol. 17.* World Scientific Publishing, Singapore. Advanced Series on Ocean Engineering.

Temel, A., & Dogan, M. (2021). Time-dependent investigation of the wave induced scour at the trunk section of a rubble mound breakwater. *Ocean Engineering*, *221*, 108564.

Xie, S. L. (1981). *Scouring patterns in front of vertical breakwaters and their influences on the stability of the foundation of the breakwaters.* PhD Thesis, TU Delft, Netherlands, 121.

Yalin, M. S., & Karahan, E. (1979). Inception of sediment transport. *Journal of the hydraulics division*, *105*(11), 1433-1443.